Supporting information

A reversibly photoresponsive halogen bonding receptor as a photoswitchable catalyst for an anion abstraction reaction and cationic polymerization

Qi Jin, Yu Hai, Li-Juan Liu,* Tian-Guang Zhan and Kang-Da Zhang*

Key Laboratory of the Ministry of Education for Advanced Catalysis Materials, College of Chemistry and Materials Science, Zhejiang Normal University, 688 Yingbin Road, Jinhua 321004, China.

E-mails: lijuanliu@zjnu.edu.cn, Kangda.Zhang@zjnu.cn

Table of Contents

Section 1: Experimental and materials

All the chemical reagents were used as received from the commercial suppliers and used without further purification. Compound **4**[1] was synthesized according to the previously reported procedures.

Nuclear Magnetic Resonance (NMR) spectroscopy: The solution phase ^{1}H NMR and ^{13}C NMR spectra were recorded on a Bruker AVANCE 400 and 600 spectrometers, and the chemical shifts (δ in ppm) were determined with a residual proton of the solvent as standard.

UV-Vis absorption spectroscopy: The UV-Vis spectra were recorded on an Agilent Technologies Cary 60 UV-Vis spectrometer.

Section 2: Synthesis of receptor XB-1

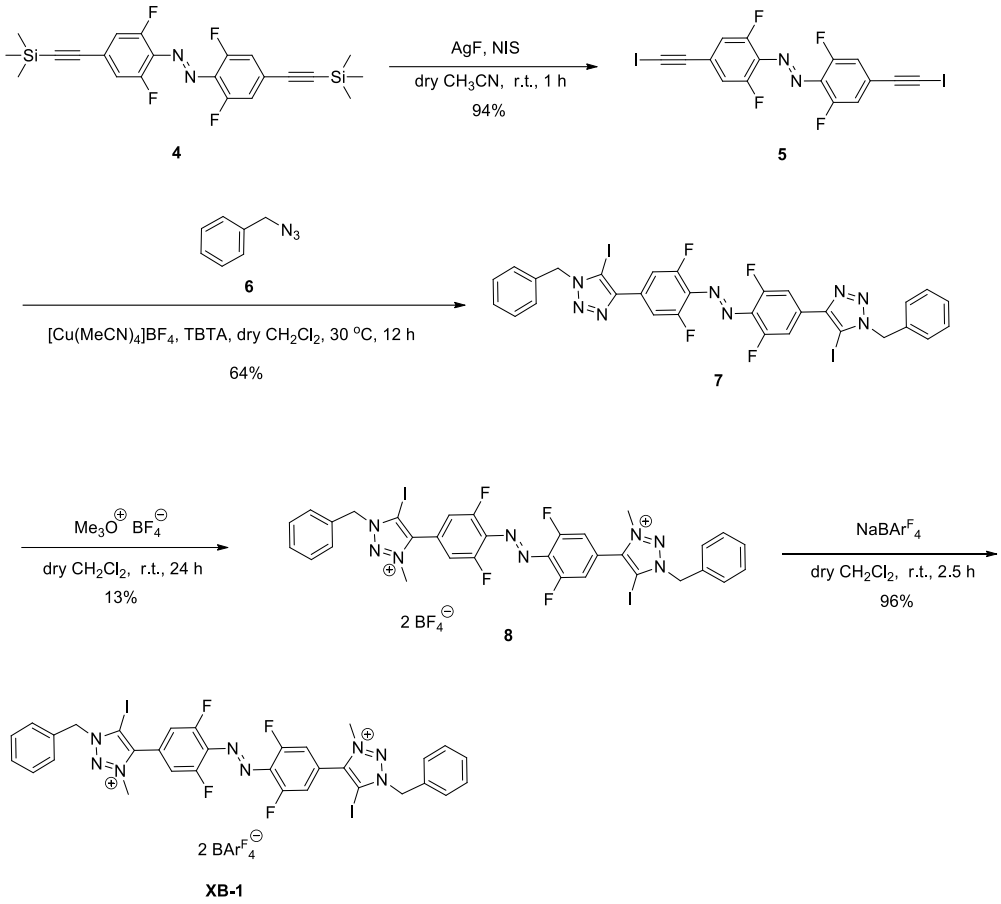

Scheme S1. The synthetic route for receptor **XB-1**.

Synthesis of compound 5. To a solution of compound **4**[1] (1.51 g, 3.39 mmol) in dry CH_3CN was added AgF (0.950 g, 7.48 mmol), N-Iodosuccinimide (NIS) (1.71 g, 7.60 mmol), the resulting mixture was deoxygenated by bubbling nitrogen gas for 10 min, after which it was allowed to be stirred at room temperature. When the TLC suggested the reaction was completed, the reaction mixture was concentrated *via* evaporation under reduced pressure to remove the solvent. Then, the residue was washed by water to remove the remaining AgF salt, and the obtained crude was finally purified by flash column chromatography eluted by petroleum ether to afford compound **5** as orange-red solid (1.76 g, 94%)

^{1}H NMR (400 MHz, DMSO-d_6, 298 K) δ: 7.50 (d, J = 10.0 Hz, 4H). ^{13}C NMR (150 MHz, DMSO-d_6, 298 K) δ: 155.03 (dd, J_1 = 258.9 Hz, J_2 = 5.3 Hz), 131.42 (t, J = 9.8 Hz), 127.74 (t, J = 12.8 Hz), 117.42 (dd, J_1 = 21.8 Hz, J_2 = 3.6 Hz), 90.94, 27.34. ^{19}F NMR (376 MHz, DMSO-d_6, 298 K) δ: -120.48. HRMS (ESI) Calcd. for $C_{16}H_5F_2I_2N_2$ $[M+H]^+$: 554.8473, Found: 554.8494.

Synthesis of compound 7. To a three-necked flask was charged with compound **6** (0.531 g, 3.98 mmol) and dry CH_2Cl_2 (10 mL), compound **5** (0.977 g, 1.76 mmol), $[Cu(MeCN)_4]BF_4$ (0.246 g, 0.780 mmol) and TBTA (0.378 g, 0.710 mmol) were then added. The resulting mixture was deoxygenated through three freeze-pump-thaw cycles in liquid N_2, after which it was allowed to

warm up and kept stirring at 30°C for 24 hours until TLC suggested the reaction was completed. The reaction mixture filtrated by diatomite to remove solvent, and the collected crude solid was further submitted to flash column chromatography for purification by using a binary solvent of CH_2Cl_2/CH_3OH = 100/1 as eluent, which finally give compound **7** as orange-red solid (0.920 g, 64%).

^{1}H NMR (400 MHz, DMF-d_7, 298 K) δ: 8.14 (d, J = 10.8 Hz, 4H), 7.49-7.39 (m, 10H), 5.91 (s, 4H). ^{13}C NMR (150 MHz, DMF-d_7, 298 K) δ: 155.77 (dd, J_1 = 258.2 Hz, J_2 = 4.5 Hz), 146.41, 135.78 (t, J = 10.8 Hz), 135.55, 130.71, 129.15, 128.53, 127.91, 111.02 (dd, J_1 = 22.2 Hz, J_2 = 3.3 Hz), 82.66, 54.21. ^{19}F NMR (376 MHz, DMF-d_7, 298 K) δ ppm: -120.60. HRMS (ESI) Calcd. for $C_{30}H_{19}F_4I_2N_8$ $[M+H]^+$: 820.9753, Found: 820.9734.

Synthesis of compound 8. A glass tube was charged with compound **7** (0.100 g, 0.122 mmol), $Me_3O^+BF_4^-$ (0.437 g, 0.295 mmol) and dry CH_2Cl_2 (2.5 mL), after which the glass tube was sealed and stirred at room temperature for 24 hours. The reaction mixture was concentrated by evaporation under reduced pressure, the remained crude was then washed by THF for several times to remove the mono-substituted triazole derivative. The obtained solid was further dissolved in the minimum amount of acetonitrile and added dropwise to diethyl ether to re-precipitate, which was collected and dried to afford compound **8** as light orange solid (0.0160 g, 13%).

^{1}H NMR (600 MHz, CD_3CN, 298 K) δ: 7.53-7.49 (m, 10H), 7.45 (d, J = 9.0 Hz, 4H), 5.87 (s, 4H), 4.21 (s, 6H). ^{13}C NMR (150 MHz, CD_3CN, 298 K) δ: 155.42 (dd, J_1 = 261.0 Hz, J_2 = 4.4 Hz), 144.59, 133.09 (t, J = 9.8 Hz), 131.40, 129.64, 129.20, 129.08, 126.57 (t, J = 11.4 Hz), 115.72 (dd, J_1 = 21.9 Hz, J_2 = 4.5 Hz), 90.37, 58.10, 39.50. ^{19}F NMR (564 MHz, CD_3CN, 298 K) δ: -119.49, -151.83 (d). HRMS (ESI) Calcd. for $C_{32}H_{24}F_4I_2N_8$ $[M\text{-}2\ BF_4^-]^{2+}$: 425.0069, Found: 425.0072.

Synthesis of compound XB-1. To a glass tube was charged with compound **8** (0.0670 g, 0.0654 mmol), sodium tetrakis[3,5-bis(trifluoromethyl)phenyl]borate hydrate ($NaBAr^F{}_4$) (0.117 g, 0.132 mmol) and dry CH_2Cl_2 (3.0 mL), the tube was sealed and then keep stirring at room temperature for 2.5 hours. Water was added to the reaction mixture and then extracted by CH_2Cl_2 (20 mL×2), the organic layer was dried by anhydrous Na_2SO_4, which was further removed by filtration. The filtrate was concentrated via evaporation under reduced pressure, the received solid residue was further dissolved in CH_2Cl_2 (2 mL), and the solution was then added into n-hexane (5 mL) to regenerate precipitates, which was collected by filtration and dried under vacuum to give compound **XB-1** as orange solid (0.162 g, 96%). ^{1}H NMR (400 MHz, CD_2Cl_2, 298 K) δ: 7.72 (s, 16H), 7.59-7.54 (m, 18H), 7.27 (d, J = 7.6 Hz, 4H), 5.88 (s, 4H), 4.34 (s, 6H). ^{13}C NMR (150 MHz, CD_3CN, 298 K) δ: 161.62 (q, J = 49.5 Hz), 155.45 (dd, J_1 = 261.5 Hz, J_2 = 4.7 Hz), 144.62, 134.66, 133.09 (t, J = 10.5 Hz), 131.31, 129.70, 129.20, 129.11, 126.43 (qdd, J_1 = 31.1 Hz, J_2 = 5.7 Hz, J_3 = 2.7 Hz), 126.43 (t, J = 11.3 Hz), 124.47 (q, J = 270.2 Hz), 117.74-117.60 (m), 115.65 (dd, J_1 = 21.9 Hz, J_2 = 4.8 Hz), 90.44, 58.16, 39.53. ^{19}F NMR (376 MHz, CD_2Cl_2, 298 K) δ: -62.80, -115.37. HRMS (ESI) Calcd. for $C_{32}H_{24}F_4I_2N_8$ $[M\text{-}2BAr^F{}_4^-]^{2+}$: 425.0069, Found: 425.0074.

Section 3: The photoisomerization property and photoswitchable halogen bonding behavior of receptor XB-1

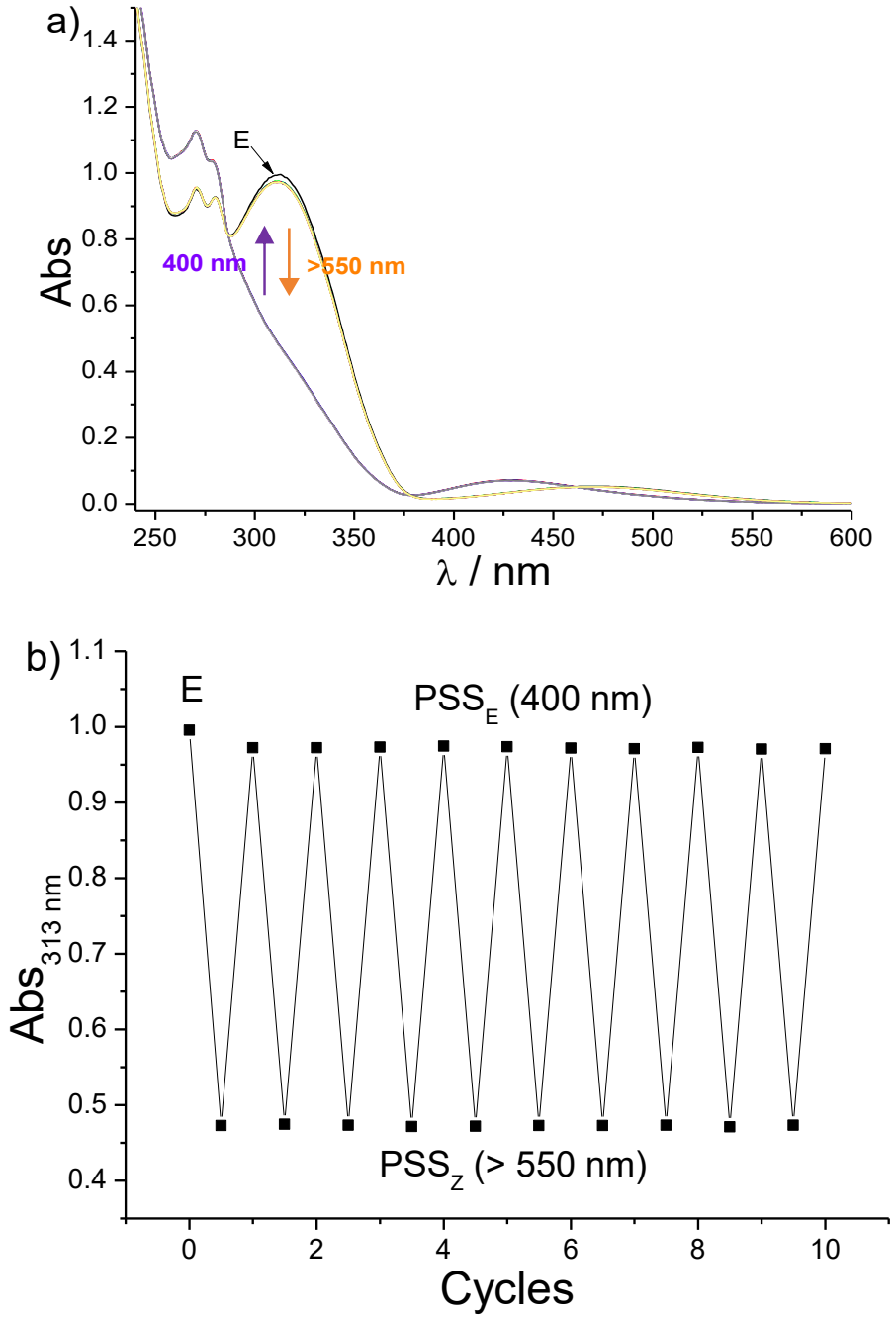

Fig. S1 a) UV-Vis absorption spectra (in CH_2Cl_2 at 25 °C) of **XB-1** (0.10 mM), and b) plot of corresponding absorption λ at 313 nm after purple light irradiation (λ = 400 nm), and purple light-irradiated **XB-1** solution after yellow light (λ > 550 nm) irradiation before next light irradiation.

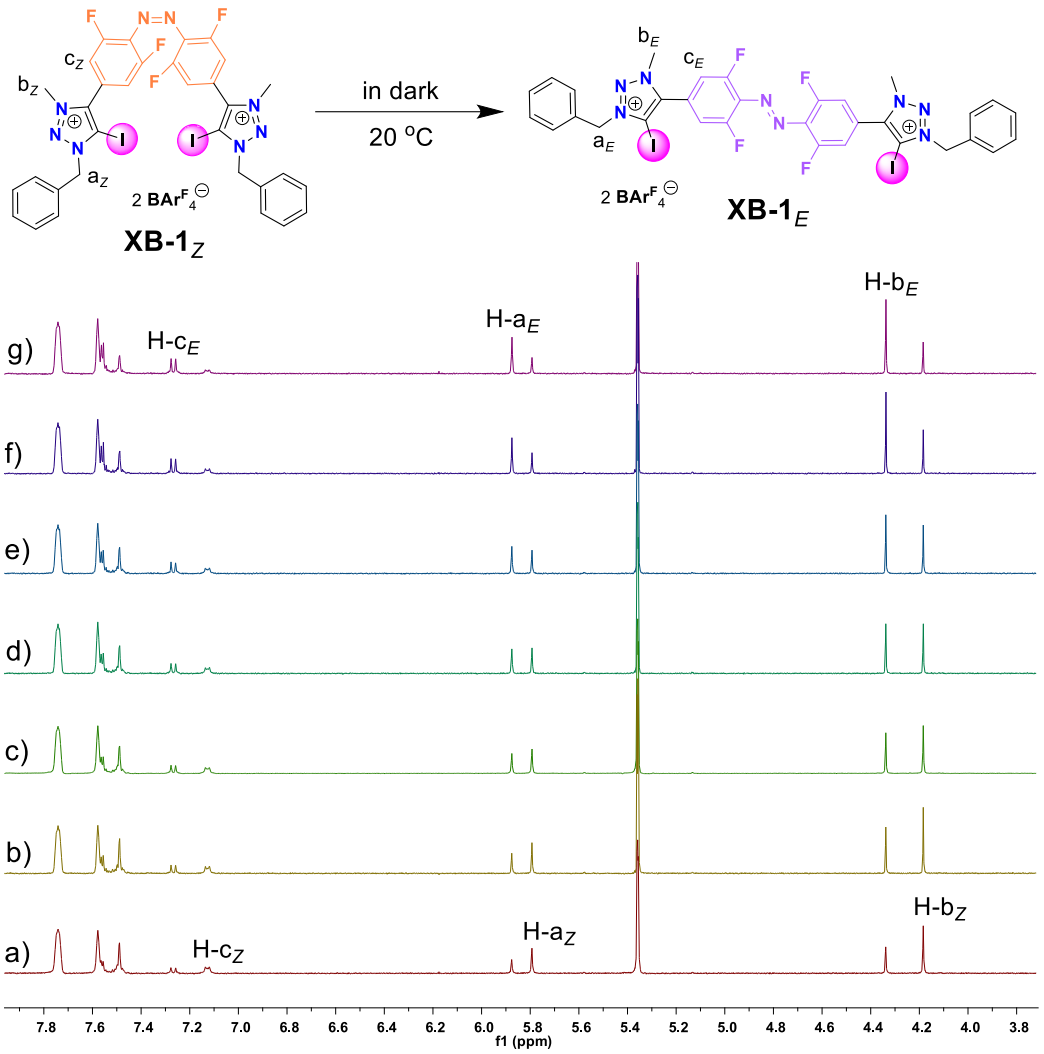

Fig. S2 Schematic representation of the *Z*-to-*E* thermal relaxation behavior of **XB-1**, and the ^{1}H NMR spectra (400 MHz, 2.0 mM, CD_2Cl_2, 298 K) for the solution of the PSS$_Z$ (>550 nm) mixtures of **XB-1** under conditions of a) as prepared, and after the rest of b) 1 d, c) 2 d, d) 3 d, e) 4 d, f) 7 d, and g) 9 d at 20 °C in dark.

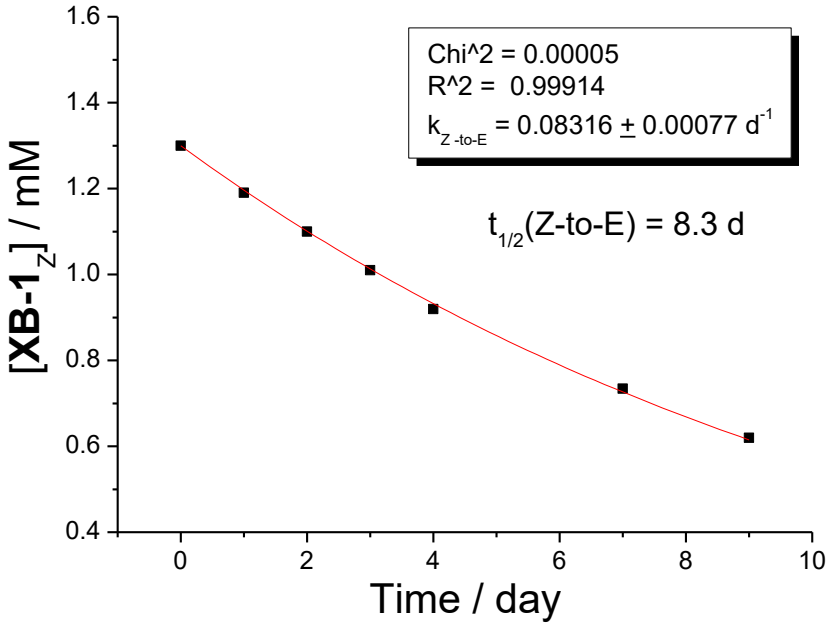

Fig. S3 Time dependent concentration change plots and the fitting curve of **XB-1**$_Z$ at 20 °C in dark. The concentration of **XB-1**$_Z$ is determined based on the integral ratios of H-a$_Z$ and H-a$_E$ in Fig.S2.

The rate of the isomers of **XB-1**$_E$ and **XB-1**$_Z$ at the PSS$_E$ (400 nm) was also calculated based on the combination of their UV-Vis and ^{1}H NMR spectra before and after light irradiation, with the following notes:

(1) $A_{313\ nm}$ corresponds to the absorbance at 313 nm of the solution of **XB-1**.

(2) ε_E (313 nm) is the molar extinction coefficient of the absorption band at 313 nm of **XB-1**$_E$.

(3) ε_Z (313 nm) is the molar extinction coefficient of the absorption band at 313 nm of **XB-1**$_Z$.

(4) The contents of **XB-1**$_E$ and **XB-1**$_Z$ in the $PSS_{>550\ nm}$ mixtures solution were determined as 35% and 65 % based on the ^{1}H NMR results, respectively.

The detailed calculation is described as follows in Fig. S4:

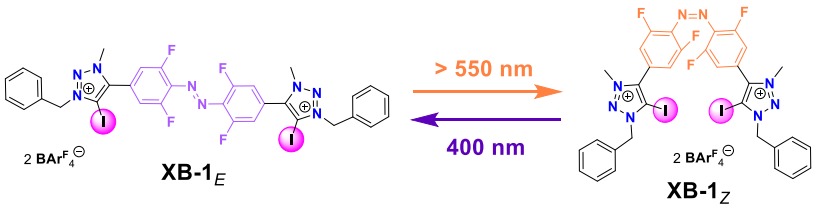

Before irradiation:	C_0	0
At $PSS_{>550\ nm}$:	$C_E(PSS_{>550\ nm})$	$C_Z(PSS_{>550\ nm})$
At $PSS_{400\ nm}$:	$C_E(PSS_{400\ nm})$	$C_Z(PSS_{400\ nm})$

Before irradiation with light light:

$$A_{313\ nm}(E) = C_0 \times \varepsilon_E(313\ nm)$$

After yellow (>550 nm) light irradiation:

$$A_{313\ nm}(PSS_{>550\ nm}) = C_E(PSS_{>550\ nm}) \times \varepsilon_E(313\ nm) + C_Z(PSS_{>550\ nm}) \times \varepsilon_Z(313\ nm)$$
$$= C_0 \times \{ [C_E(PSS_{>550\ nm})/C_0] \times \varepsilon_E(313\ nm) + [C_Z(PSS_{>550\ nm})/C_0] \times \varepsilon_Z(313\ nm) \}$$
$$= C_0 \times [0.35 \times \varepsilon_E(313\ nm) + 0.65 \times \varepsilon_Z(313\ nm)]$$

$$A_{313\ nm}(PSS>_{550\ nm}) / A_{313\ nm}(E) = C_0 \times \{ [\,0.35 \times \varepsilon_E(313\ nm) + 0.65 \times \varepsilon_Z(313\ nm)\,] \} / [C_0 \times \varepsilon_E(313\ nm)]$$
$$= [0.35 \times \varepsilon_E(313\ nm) + 0.65 \times \varepsilon_Z(313\ nm)] / \varepsilon_E(313\ nm)$$

$$\varepsilon_Z(313\ nm) = \{ [A_{313\ nm}(PSS>_{550\ nm}) / A_{313\ nm}(E)] \times \varepsilon_E(313\ nm) - 0.35 \times \varepsilon_E(313\ nm) \} / 0.65$$
$$= \{ [0.473 / 0.995] \times \varepsilon_E(313\ nm) - 0.35 \times \varepsilon_E(313\ nm) \} / 0.65$$
$$= 0.19 \times \varepsilon_E(313\ nm)$$

After purple (400 nm) light irradiation:

$$A_{313\ nm}(PSS_{400\ nm}) = C_E(PSS_{400\ nm}) \times \varepsilon_E(313\ nm) + C_Z(PSS_{400\ nm}) \times \varepsilon_Z(313\ nm)$$
$$= C_0 \times \{ [C_E(PSS_{400\ nm})/C_0] \times \varepsilon_E(313\ nm) + [C_Z(PSS_{400\ nm})/C_0] \times \varepsilon_Z(313\ nm) \}$$
$$= C_0 \times \{ [C_E(PSS_{400\ nm})/C_0] \times \varepsilon_E(313\ nm) + [C_Z(PSS_{400\ nm})/C_0] \times 0.19 \times \varepsilon_E(313\ nm) \}$$
$$= C_0 \times \varepsilon_E(313\ nm) \times \{ [C_E(PSS_{400\ nm})/C_0] + [C_Z(PSS_{400\ nm})/C_0] \times 0.19 \}$$
$$= C_0 \times \varepsilon_E(313\ nm) \times \{ 1 - [C_Z(PSS_{400\ nm})/C_0] + [C_Z(PSS_{400\ nm})/C_0] \times 0.19 \}$$
$$= C_0 \times \varepsilon_E(313\ nm) \times \{ 1 - [C_Z(PSS_{400\ nm})/C_0] \times 0.81 \}$$

$$C_Z(PSS_{400\ nm}) / C_0 = \{ 1 - [A_{313\ nm}(PSS_{400\ nm}) / C_0 \times \varepsilon_E(313\ nm)] \} / 0.81$$
$$= [1 - A_{313\ nm}(PSS_{400\ nm}) / A_{313\ nm}(E)] / 0.81$$
$$= [1 - 0.973 / 0.995] / 0.81$$
$$= 0.027$$

Fig. S4 The detailed calculation procedures for the distributions of **XB-1**$_E$ and **XB-1**$_Z$ at PSS_E (400 nm). Note: the ratio of **XB-1**$_E$ and **XB-1**$_Z$ at PSS_E (400 nm) obtained by this UV-Vis based method is consistent with that calculated based on the ^{1}H NMR data.

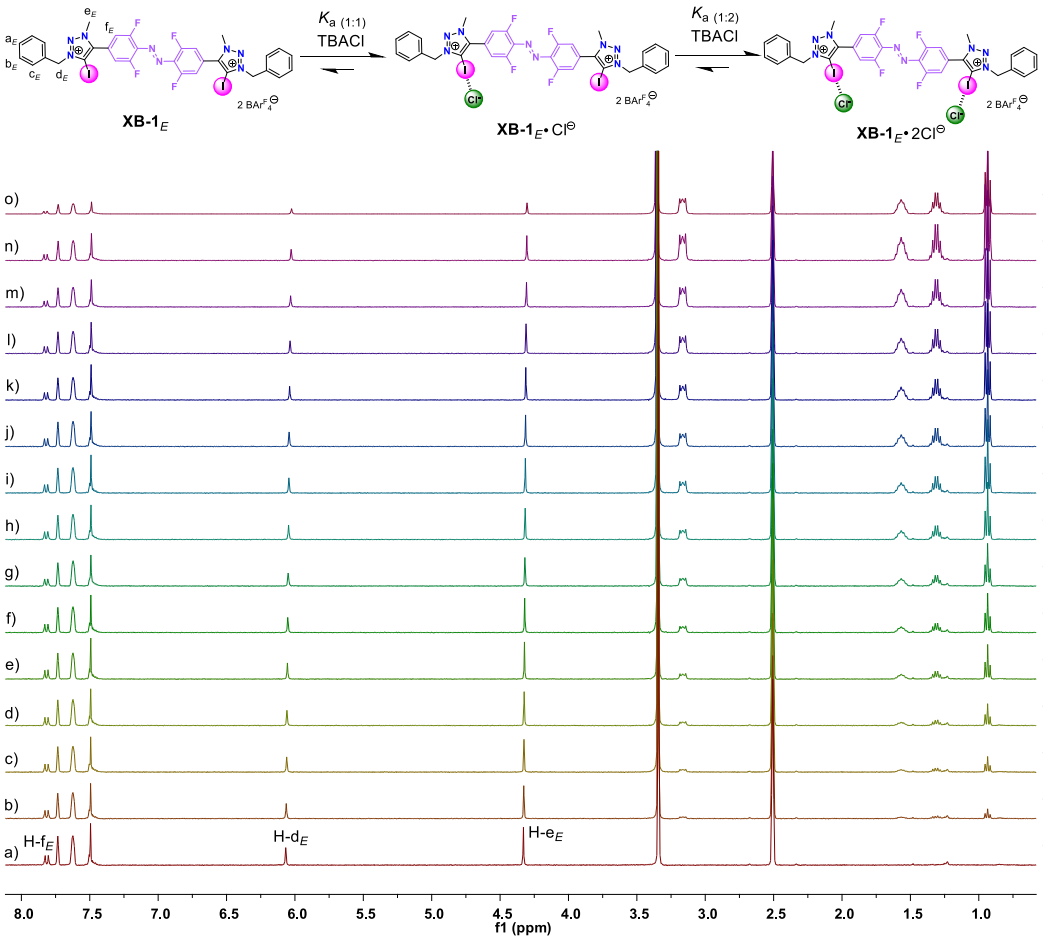

Fig. S5 Schematic representation for the complexation between **XB-1**$_E$ and TBACl, and ^{1}H NMR spectra (400 MHz, DMSO-d_6, 298 K) for the solution of **XB-1**$_E$ (2.0 mM) in the presence of a) 0, b) 0.28, c) 0.45, d) 0.60, e) 0.87, f) 1.1, g) 1.4, h) 1.7, i) 2.0, j) 2.2, k) 2.8, l) 3.3, m) 4.4, n) 5.5 and o) 6.7 equiv. of TBACl.

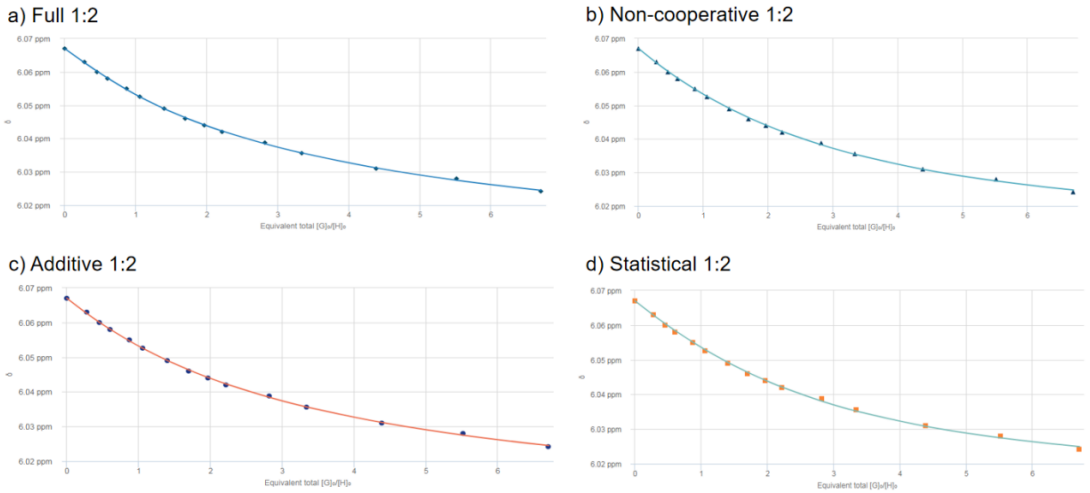

Fig. S6 The plot of chemical shifts for the proton signal H-d$_E$ of **XB-1**$_E$ *versus* the ratios of TBACl / **XB-1**$_E$ in DMSO-d_6 at 298 K, with the solid line representing the non-linear regression fitting of the data to the different 1:2 binding models.[2]

Table S1. Association constants for receptor **XB-1**$_E$ binding with the chloride anion determined based on the ^{1}H NMR titration spectra (400 MHz, 298 K) of **XB-1**$_E$ (2.0 mM) with TBACl in DMSO-d_6. Different 1:2 binding models were compared and the appropriate binding model was highlighted in blue.

Binding models	cov_{fit} (10^{-3})	cov_{fit} factor [a]	$K_{a\ (1:1)}$ (M^{-1})	$K_{a\ (1:2)}$ (M^{-1})
Full 1:2 ($K_{a\ (1:1)} \neq 4K_{a\ (1:2)}$) ($\delta_{\Delta HG2} \neq 2\delta_{\Delta HG}$)	0.406	2.46	2669 (± 14.9%) [b]	115 (± 3.8%) [b]
Non-cooperative 1:2 ($K_{a\ (1:1)} = 4K_{a\ (1:2)}$) ($\delta_{\Delta HG2} \neq 2\delta_{\Delta HG}$)	0.609	1.64	313 (± 2.2%) [b]	78
Additive 1:2 ($K_{a\ (1:1)} \neq 4K_{a\ (1:2)}$) ($\delta_{\Delta HG2} = 2\delta_{\Delta HG}$)	0.461	2.17	524 (± 5.4%) [b]	73 (± 6.6%) [b]
Statistical 1:2 ($K_{a\ (1:1)} = 4K_{a\ (1:2)}$) ($\delta_{\Delta HG2} = 2\delta_{\Delta HG}$)	1.00	1.0	633 (± 3.2%) [b]	158

[a] cov_{fit} factor = cov_{fit} for the statistical 1:2 binding model divided by the cov_{fit} for the binding model under study.

[b] The values in parentheses are the errors of the binding constants obtained by fitting.

Conclusion: The cov_{fit} values of full 1:2, non-cooperative 1:2, additive 1:2 and statistical 1:2 binding model are very close. However, when a more complex binding model is selected, the selection is justified by an improved cov_{fit} factor (> 3-5 fold) than the less complex model[3]. Hence, we conclude that the statistical 1:2 binding model is the appropriate binding model.

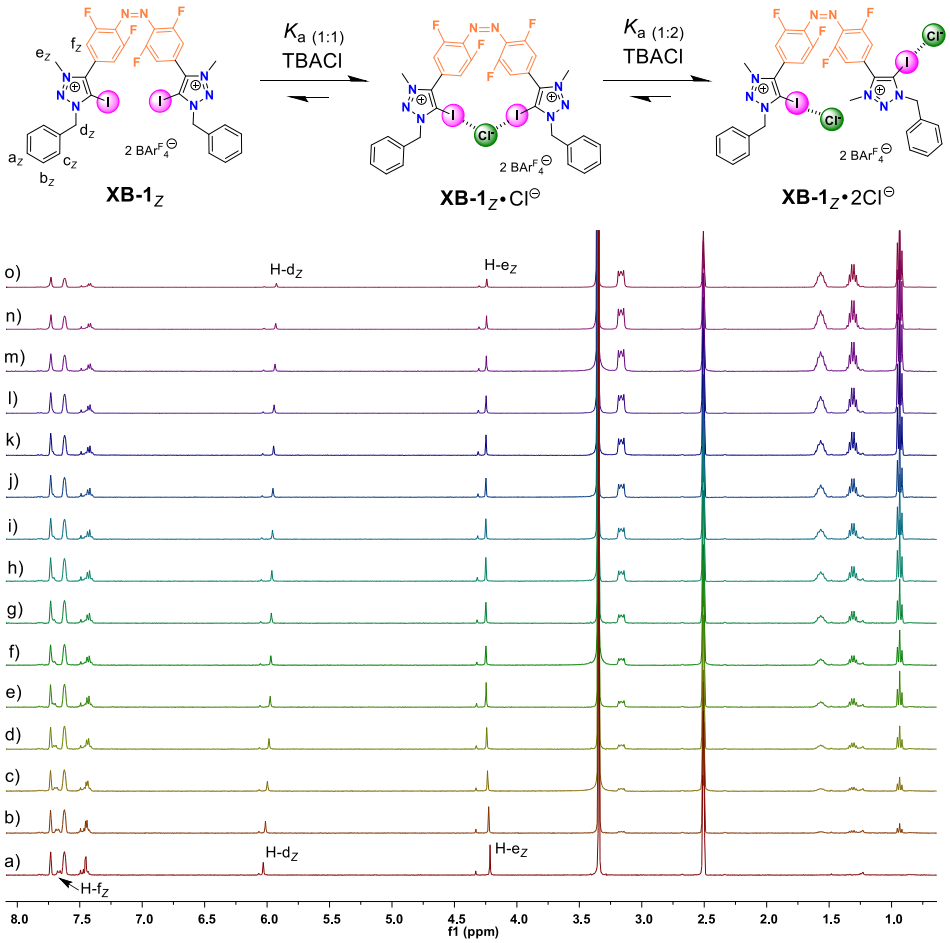

Fig. S7 Schematic representation for the complexation between **XB-1**$_Z$ and TBACl, and ^{1}H NMR spectra (400 MHz, DMSO-d_6, 298 K) for the PSS$_Z$ (>550 nm) mixtures of **XB-1** (2.0 mM) in the presence of a) 0, b) 0.30, c) 0.56, d) 0.83, e) 1.1, f) 1.4, g) 1.7, h) 2.0, i) 2.5, j) 2.9, k) 3.6, l) 4.2, m) 5.6, n) 6.6 and o) 8.1 equiv. of TBACl.

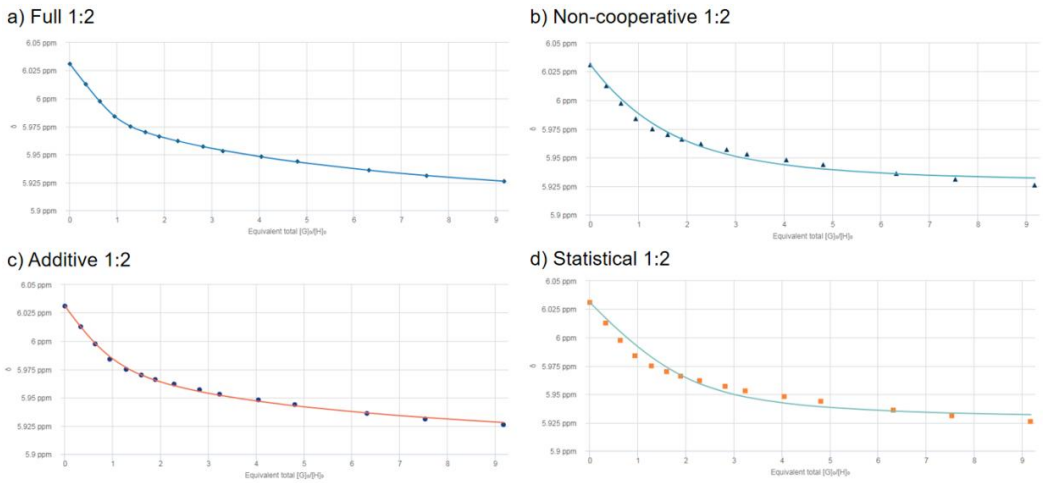

Fig. S8 The plot of chemical shifts for the proton signal H-d$_Z$ of **XB-1**$_Z$ *versus* the ratios of TBACl / **XB-1**$_Z$ in DMSO-d_6 at 298 K, with the solid line representing the non-linear regression fitting of the data to the different 1:2 binding models.[2]

Table S2. Association constants for receptor **XB-1**$_Z$ binding with the chloride anion determined based on the ^{1}H NMR titration spectra (400 MHz, 298 K) of the PSS$_Z$ (>500 nm) mixtures of **XB-1** (2.0 mM) with TBACl in DMSO-d_6. Different 1:2 binding models were compared and the appropriate binding model was highlighted in blue.

Binding models	cov_{fit} (10^{-3})	cov_{fit} factor [a]	$K_{a\ (1:1)}$ (M^{-1})	$K_{a\ (1:2)}$ (M^{-1})
Full 1:2 ($K_{a\ (1:1)} \neq 4K_{a\ (1:2)}$) ($\delta_{\Delta HG2} \neq 2\delta_{\Delta HG}$)	0.0601	502	15270 (± 9.2%) [b]	89 (± 1.3%) [b]
Non-cooperative 1:2 ($K_{a\ (1:1)} = 4K_{a\ (1:2)}$) ($\delta_{\Delta HG2} \neq 2\delta_{\Delta HG}$)	15.3	1.97	872 (± 17.1%) [b]	218
Additive 1:2 ($K_{a\ (1:1)} \neq 4K_{a\ (1:2)}$) ($\delta_{\Delta HG2} = 2\delta_{\Delta HG}$)	1.66	18.2	2895 (± 15.3%) [b]	70 (± 8.9%) [b]
Statistical 1:2 ($K_{a\ (1:1)} = 4K_{a\ (1:2)}$) ($\delta_{\Delta HG2} = 2\delta_{\Delta HG}$)	30.2	1.0	2677 (± 30.5%) [b]	669

[a] cov_{fit} factor = cov_{fit} for the statistical 1:2 binding model divided by the cov_{fit} for the binding model under study.

[b] The values in parentheses are the errors of the binding constants obtained by fitting.

Conclusion: Based on both the cov_{fit} and inspection of the binding isotherms, the full 1:2 binding model can describe this data significantly better than all the other binding models. Hence, we conclude that the full 1:2 binding model describes this data best.

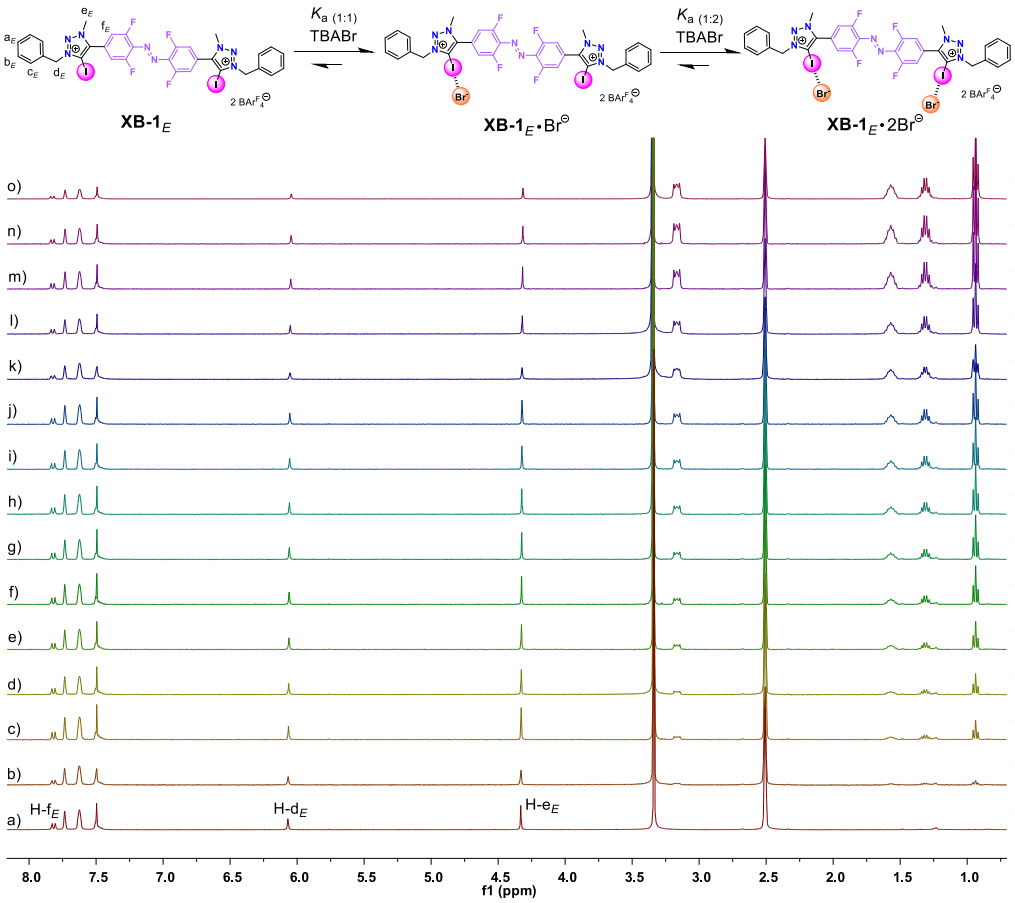

Fig. S9 Schematic representation for the complexation between **XB-1**$_E$ and TBABr, and ^{1}H NMR spectra (400 MHz, DMSO-d_6, 298 K) for the solution of **XB-1**$_E$ (2.0 mM) in the presence of a) 0, b) 0.27, c) 0.50, d) 0.70, e) 0.96, f) 1.2, g) 1.4, h) 1.7, i) 1.9, j) 2.2, k) 2.8, l) 3.3, m) 4.4, n) 5.4 and o) 6.0 equiv. of TBABr.

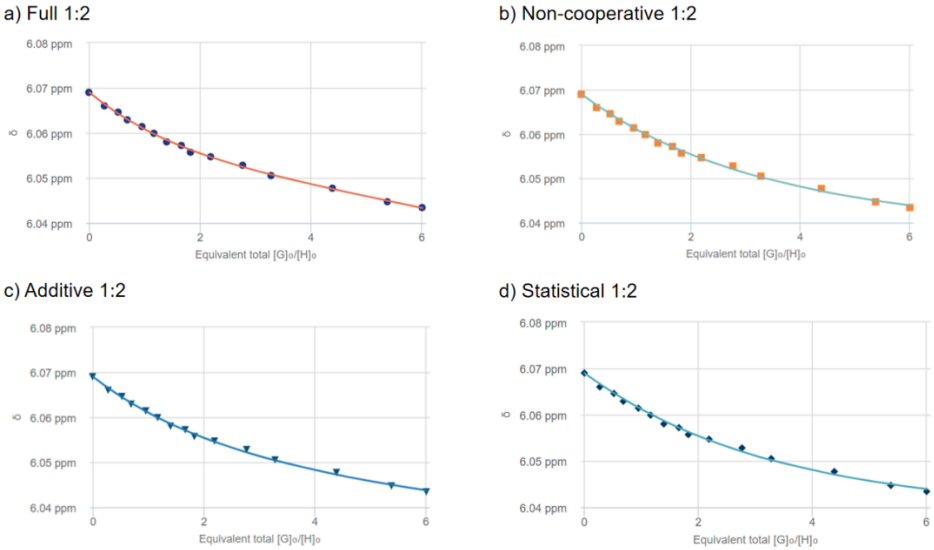

Fig. S10 The plot of chemical shifts for the proton signal H-d$_E$ of **XB-1**$_E$ *versus* the ratios of TBABr / **XB-1**$_E$ in DMSO-d_6 at 298 K, with the solid line representing the non-linear regression fitting of the data to the different 1:2 binding models.[2]

Table S3. Association constants for receptor **XB-1**$_E$ binding with the bromide anion determined based on the ^{1}H NMR titration spectra (400 MHz, 298 K) of **XB-1**$_E$ (2.0 mM) with TBABr in DMSO-d_6. Different 1:2 binding models were compared and the appropriate binding model was highlighted in blue, while the physically impossible result from the selected binding model was highlighted in red.

Binding models	cov_{fit} (10^{-3})	cov_{fit} factor [a]	$K_{a\ (1:1)}$ (M^{-1})	$K_{a\ (1:2)}$ (M^{-1})
Full 1:2 ($K_{a\ (1:1)} \neq 4K_{a\ (1:2)}$) ($\delta_{\Delta HG2} \neq 2\delta_{\Delta HG}$)	1.37	2.58	259 (± 4.8%)	-27 (± -10.9%)
Non-cooperative 1:2 ($K_{a\ (1:1)} = 4K_{a\ (1:2)}$) ($\delta_{\Delta HG2} \neq 2\delta_{\Delta HG}$)	2.87	1.23	245 (± 2.2%) [b]	61
Additive 1:2 ($K_{a\ (1:1)} \neq 4K_{a\ (1:2)}$) ($\delta_{\Delta HG2} = 2\delta_{\Delta HG}$)	2.10	1.69	273 (± 7.6%) [b]	24 (± 22.2%) [b]
Statistical 1:2 ($K_{a\ (1:1)} = 4K_{a\ (1:2)}$) ($\delta_{\Delta HG2} = 2\delta_{\Delta HG}$)	3.54	1.0	473 (± 5.1%) [b]	118

[a] cov_{fit} factor = cov_{fit} for the statistical 1:2 binding model divided by the cov_{fit} for the binding model under study.

[b] The values in parentheses are the errors of the binding constants obtained by fitting.

Conclusion: The full 1:2 binding model is impossible as it shows a negative $K_{a\ (1:2)}$ value. The cov_{fit} values of non-cooperative 1:2, additive 1:2 and statistical 1:2 binding model are very close. However, when a more complex binding model is selected, the selection is justified by an improved cov_{fit} factor (> 3-5 fold) than the less complex model[3]. Hence, we conclude that the statistical 1:2 binding model is the appropriate binding model.

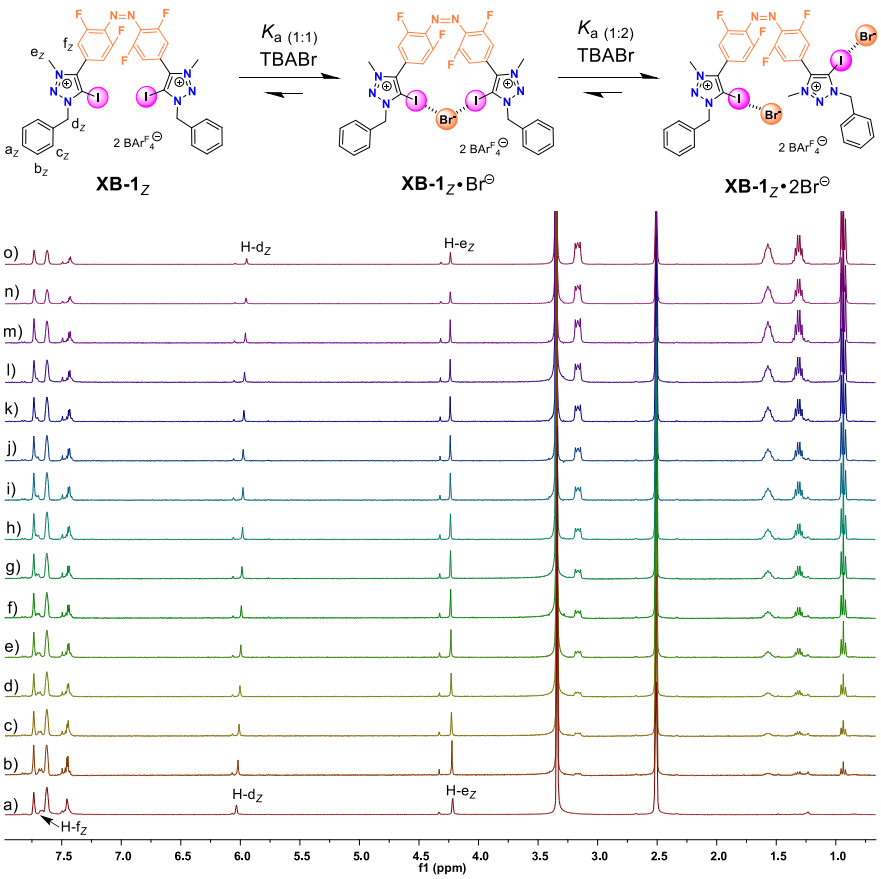

Fig. S11 Schematic representation for the complexation between **XB-1**$_Z$ and TBABr, and ^{1}H NMR spectra (400 MHz, DMSO-d_6, 298 K) for the PSS$_Z$ (>550 nm) mixtures of **XB-1** (2.0 mM) in the presence of a) 0, b) 0.28, c) 0.46, d) 0.65, e) 0.91, f) 1.1, g) 1.3, h) 1.6, i) 1.9, j) 2.1, k) 2.6, l) 3.2, m) 4.2, n) 5.2 and o) 6.2 equiv. of TBABr.

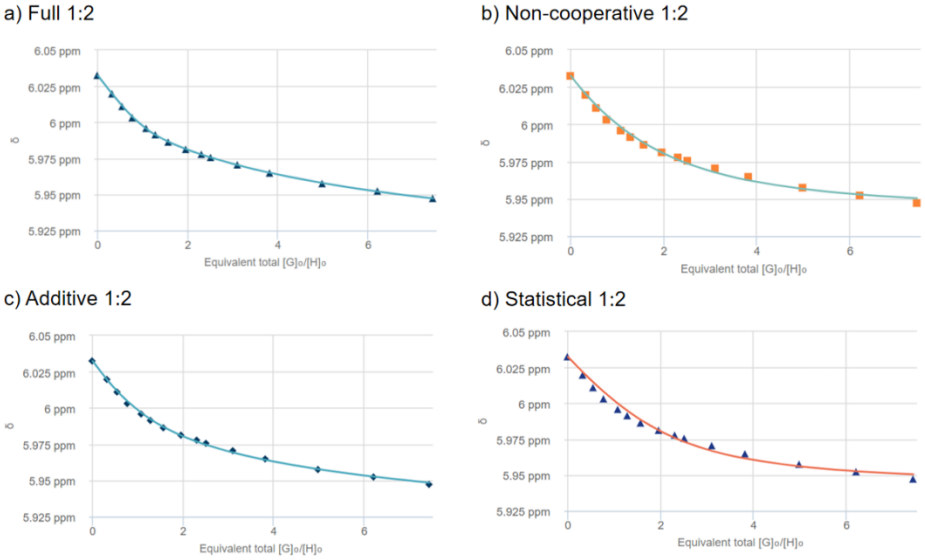

Fig. S12 The plot of chemical shifts for the proton signal H-d$_Z$ of **XB-1**$_Z$ *versus* the ratios of TBABr / **XB-1**$_Z$ in DMSO-d_6 at 298 K, with the solid line representing the non-linear regression fitting of the data to the different 1:2 binding models.[2]

Table S4. Association constants for receptor **XB-1**$_Z$ binding with the bromide anion determined based on the ^{1}H NMR titration spectra (400 MHz, 298 K) of the PSS$_Z$ (>500 nm) mixtures of **XB-1** (2.0 mM) with TBABr in DMSO-d_6. Different 1:2 binding models were compared and the appropriate binding model was highlighted in blue.

Binding models	cov_{fit} (10^{-3})	cov_{fit} factor [a]	$K_{a\,(1:1)}$ (M^{-1})	$K_{a\,(1:2)}$ (M^{-1})
Full 1:2 ($K_{a\,(1:1)} \neq 4K_{a\,(1:2)}$) ($\delta_{\Delta HG2} \neq 2\delta_{\Delta HG}$)	0.15	88	7465 (± 9.9%) [b]	97 (± 2.1%) [b]
Non-cooperative 1:2 ($K_{a\,(1:1)} = 4K_{a\,(1:2)}$) ($\delta_{\Delta HG2} \neq 2\delta_{\Delta HG}$)	6.16	2.14	635 (± 8.8%) [b]	159
Additive 1:2 ($K_{a\,(1:1)} \neq 4K_{a\,(1:2)}$) ($\delta_{\Delta HG2} = 2\delta_{\Delta HG}$)	1.24	10.6	1235 (± 8.5%) [b]	57 (± 9.5%) [b]
Statistical 1:2 ($K_{a\,(1:1)} = 4K_{a\,(1:2)}$) ($\delta_{\Delta HG2} = 2\delta_{\Delta HG}$)	13.2	1.0	1814 (± 16.2%) [b]	453

[a] cov_{fit} factor = cov_{fit} for the statistical 1:2 binding model divided by the cov_{fit} for the binding model under study.

[b] The values in parentheses are the errors of the binding constants obtained by fitting.

Conclusion: Based on both the cov_{fit} and inspection of the binding isotherms, the full 1:2 binding model can describe this data significantly better than all the other binding models. Hence, we conclude that the full 1:2 binding model describes this data best.

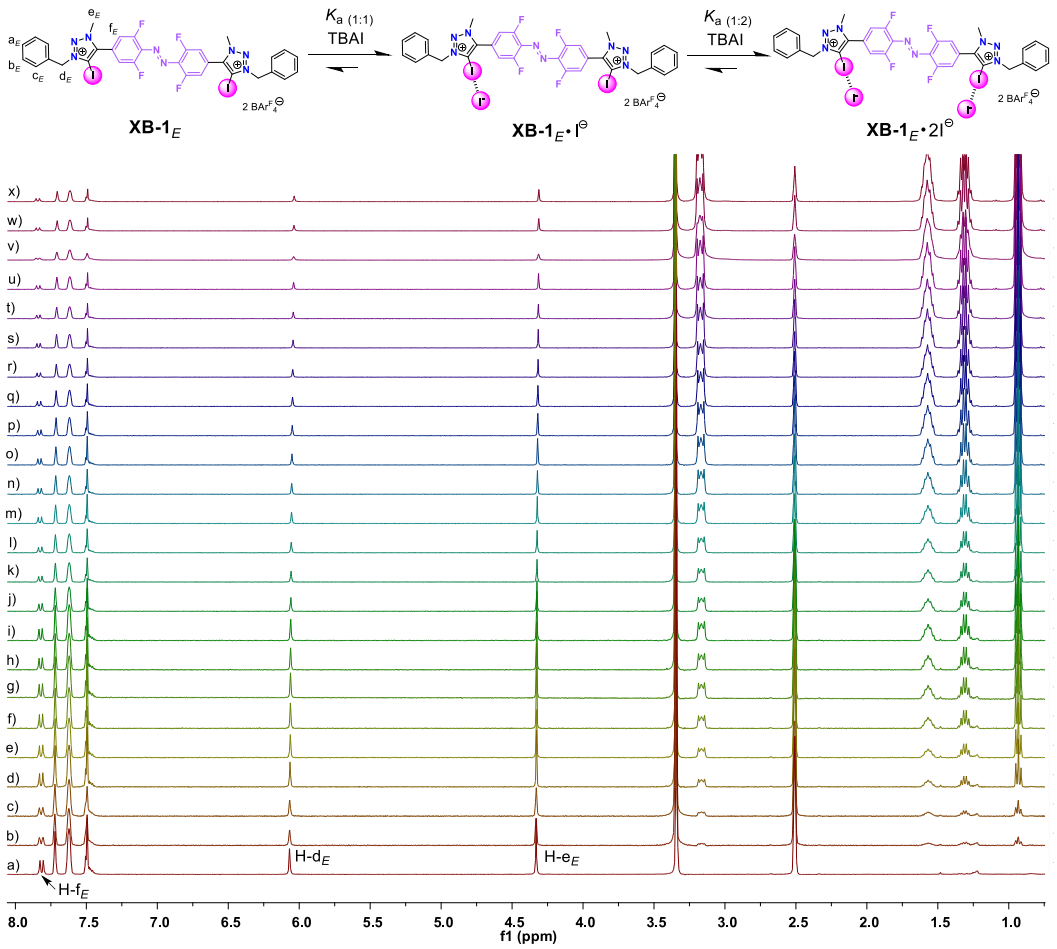

Fig. S13 Schematic representation for the complexation between **XB-1**$_E$ and TBAI, and ^{1}H NMR spectra (400 MHz, DMSO-d_6, 298 K) for the solution of **XB-1**$_E$ (2.0 mM) in the presence of a) 0, b) 0.28, c) 0.51, d) 0.75, e) 1.0, f) 1.3, g) 1.6, h) 1.9, i) 2.2, j) 2.5, k) 3.1, l) 3.6, m) 4.6, n) 5.7, o) 6.8, p) 8.1, q) 9.8, r) 12, s) 14, t) 16, u) 18, v)20, w) 21 and x) 24 equiv. of TBAI.

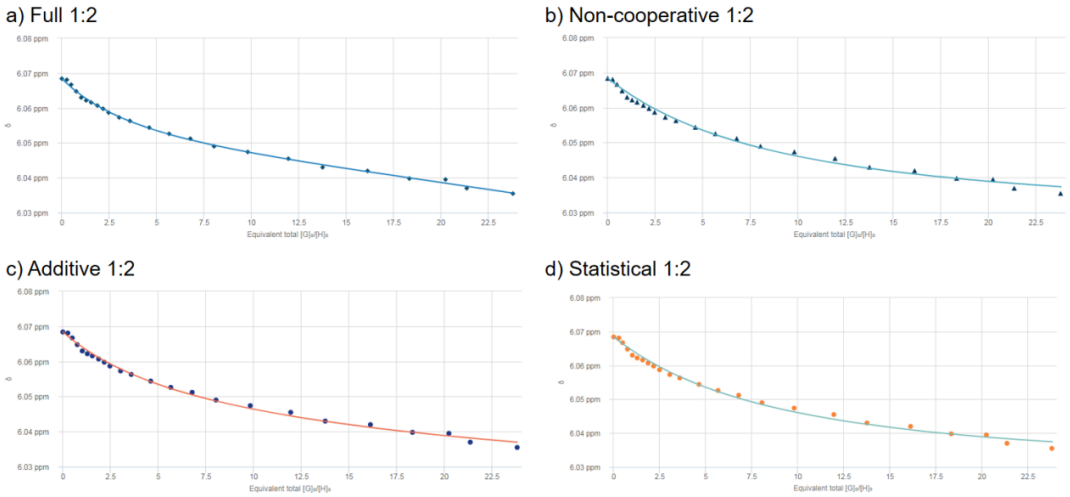

Fig. S14 The plot of chemical shifts for the proton signal H-d$_E$ of **XB-1**$_E$ *versus* the ratios of TBAI / **XB-1**$_E$ in DMSO-d_6 at 298 K, with the solid line representing the non-linear regression fitting of the data to the different 1:2 binding models.[2]

Table S5. Association constants for receptor **XB-1**$_E$ binding with the iodide anion determined based on the ^{1}H NMR titration spectra (400 MHz, 298 K) of **XB-1**$_E$ (4.0 mM) with TBAI in DMSO-d_6. Different 1:2 binding models were compared and the appropriate binding model was highlighted in blue, while the physically impossible result from the selected binding model was highlighted in red.

Binding models	cov_{fit} (10^{-3})	cov_{fit} factor [a]	$K_{a\,(1:1)}$ (M^{-1})	$K_{a\,(1:2)}$ (M^{-1})
Full 1:2 ($K_{a\,(1:1)} \neq 4K_{a\,(1:2)}$) ($\delta_{\Delta HG2} \neq 2\delta_{\Delta HG}$)	2.58	3.02	65 (± 5.5%)	-2.4 (± -6.0%)
Non-cooperative 1:2 ($K_{a\,(1:1)} = 4K_{a\,(1:2)}$) ($\delta_{\Delta HG2} \neq 2\delta_{\Delta HG}$)	7.60	1.02	53 (± 5.7) [b]	13
Additive 1:2 ($K_{a\,(1:1)} \neq 4K_{a\,(1:2)}$) ($\delta_{\Delta HG2} = 2\delta_{\Delta HG}$)	4.78	1.62	51 (± 9.2%) [b]	4.5 (± 16%) [b]
Statistical 1:2 ($K_{a\,(1:1)} = 4K_{a\,(1:2)}$) ($\delta_{\Delta HG2} = 2\delta_{\Delta HG}$)	7.78	1.0	62 (± 5.7%) [b]	16

[a] cov_{fit} factor = cov_{fit} for the statistical 1:2 binding model divided by the cov_{fit} for the binding model under study.

[b] The values in parentheses are the errors of the binding constants obtained by fitting.

Conclusion: The full 1:2 binding model is impossible as it shows a negative $K_{a(1:2)}$ value. The cov_{fit} values of non-cooperative 1:2, additive 1:2 and statistical 1:2 binding model are very close. However, when a more complex binding model was selected, the selection is justified by an improved cov_{fit} factor (> 3-5 fold) than the less complex model[3]. Hence, we conclude that the statistical 1:2 binding model is the appropriate binding model.

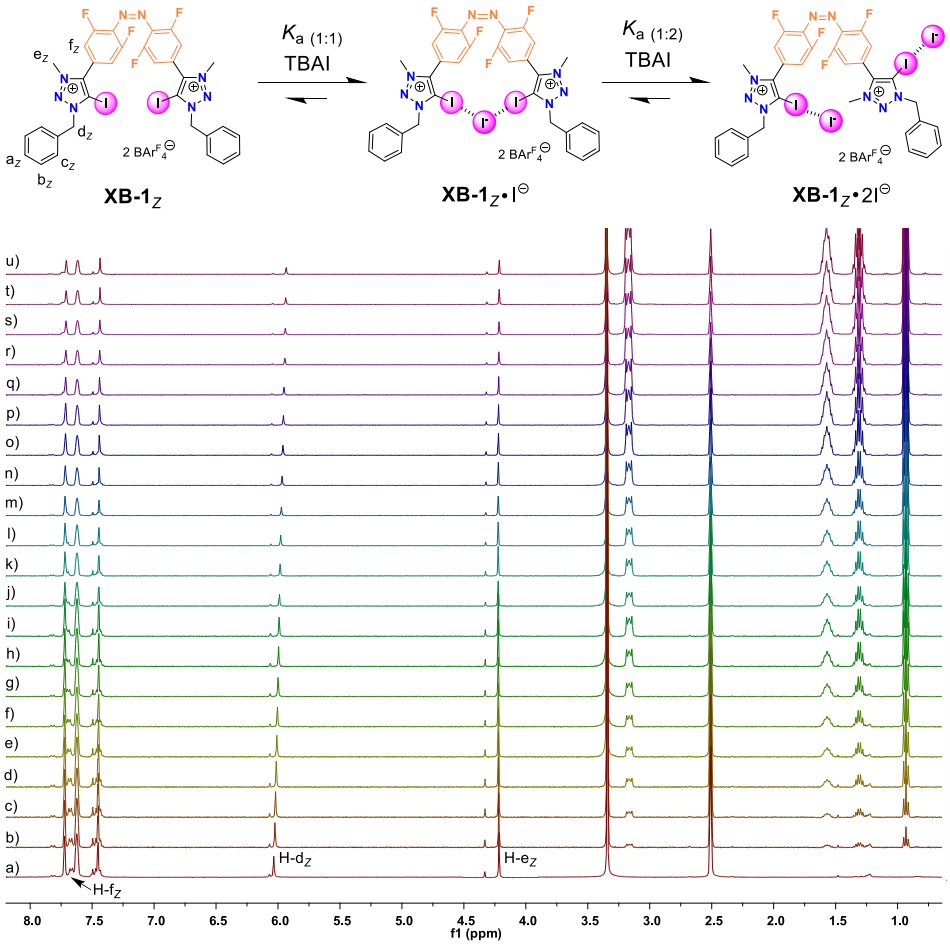

Fig. S15 Schematic representation for the complexation between **XB-1**$_Z$ and TBAI, and ^{1}H NMR spectra (400 MHz, DMSO-d_6, 298 K) for the PSS$_Z$ (>550 nm) mixtures of **XB-1** (4.0 mM) in the presence of a) 0, b) 0.32, c) 0.56, d) 0.83, e) 1.2, f) 1.4, g) 1.8, h) 2.2, i) 2.5, j) 2.9, k) 3.5, l) 4.0, m) 5.5, n) 6.6, o) 8.0, p) 9.4, q) 12, r) 13, s) 15, t) 17 and u) 18 equiv. of TBAI.

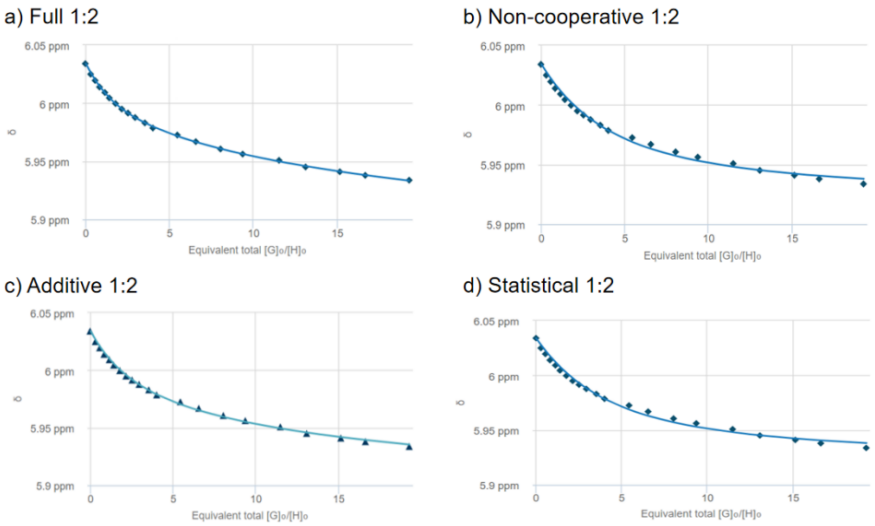

Fig. S16 The plot of chemical shifts for the proton signal H-d$_Z$ of **XB-1**$_Z$ *versus* the ratios of TBAI / **XB-1**$_Z$ in DMSO-d_6 at 298 K, with the solid line representing the non-linear regression fitting of the data to the different 1:2 binding models.[2]

Table S6. Association constants for receptor **XB-1**$_Z$ binding with the ioide anion determined based on the ^{1}H NMR titration spectra (400 MHz, 298 K) of the PSS$_Z$ (>500 nm) mixtures of **XB-1** (4.0 mM) with TBAI in DMSO-d_6. Different 1:2 binding models were compared and the appropriate binding model was highlighted in blue.

Binding models	cov_{fit} (10^{-3})	cov_{fit} factor [a]	$K_{a\,(1:1)}$ (M^{-1})	$K_{a\,(1:2)}$ (M^{-1})
Full 1:2 ($K_{a\,(1:1)} \neq 4K_{a\,(1:2)}$) ($\delta_{\Delta HG2} \neq 2\delta_{\Delta HG}$)	0.304	24.5	284 (± 3.9%) [b]	12 (± 2.2%) [b]
Non-cooperative 1:2 ($K_{a\,(1:1)} = 4K_{a\,(1:2)}$) ($\delta_{\Delta HG2} \neq 2\delta_{\Delta HG}$)	6.58	1.13	126 (± 6.6%) [b]	31
Additive 1:2 ($K_{a\,(1:1)} \neq 4K_{a\,(1:2)}$) ($\delta_{\Delta HG2} = 2\delta_{\Delta HG}$)	1.46	5.11	146 (± 5.9%) [b]	9.5 (± 7.6%) [b]
Statistical 1:2 ($K_{a\,(1:1)} = 4K_{a\,(1:2)}$) ($\delta_{\Delta HG2} = 2\delta_{\Delta HG}$)	7.46	1.0	180 (± 7.2%) [b]	45

[a] cov_{fit} factor = cov_{fit} for the statistical 1:2 binding model divided by the cov_{fit} for the binding model under study.

[b] The values in parentheses are the errors of the binding constants obtained by fitting.

Conclusion: Based on both the cov_{fit} and inspection of the binding isotherms, the full 1:2 binding model can describe this data significantly better than all the other binding models. Hence, we conclude that the full 1:2 binding model describes this data best.

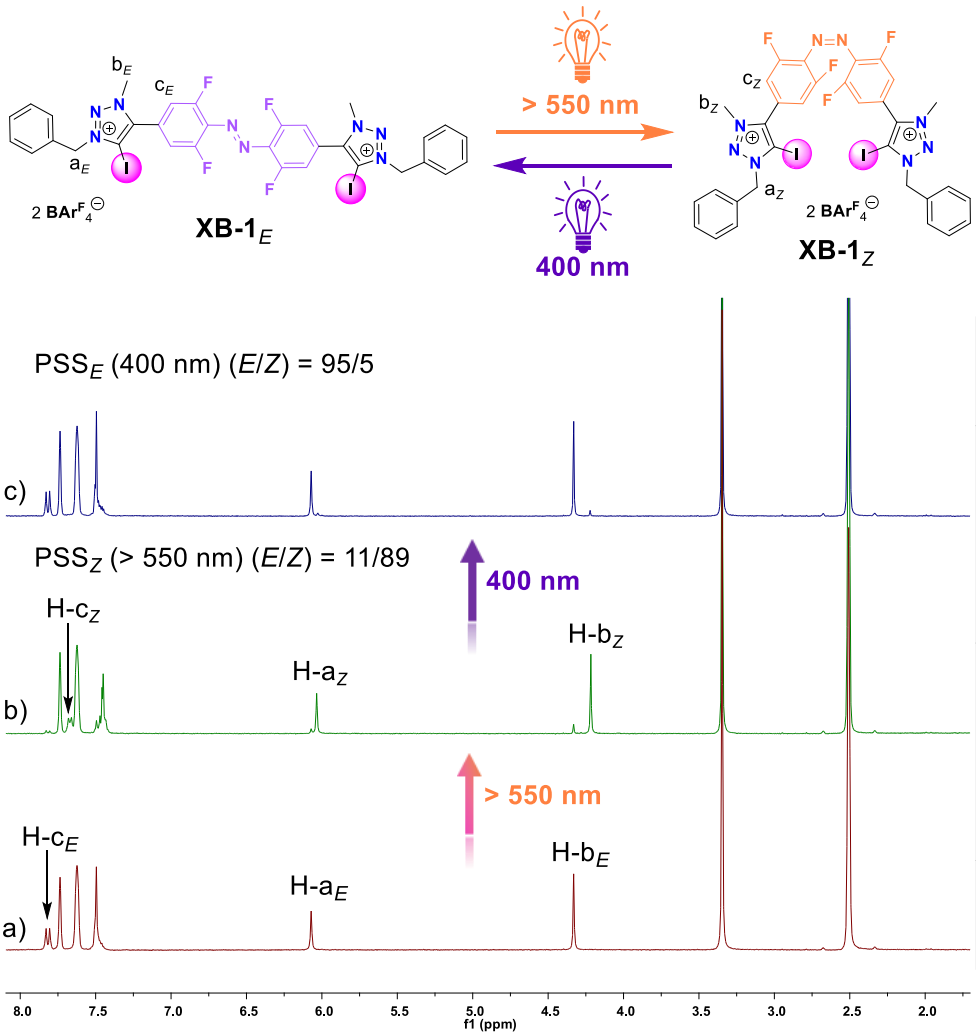

Fig. S17 ^{1}H NMR spectra (400 MHz, DMSO-d_6, 298K) for the solution of a) **XB-1**$_E$ (2.0 mM), b) the PSS$_Z$ (> 550 nm) mixtures of **XB-1** (2.0 mM), and c) the PSS$_E$ (400 nm) mixtures of **XB-1** (2.0 mM).

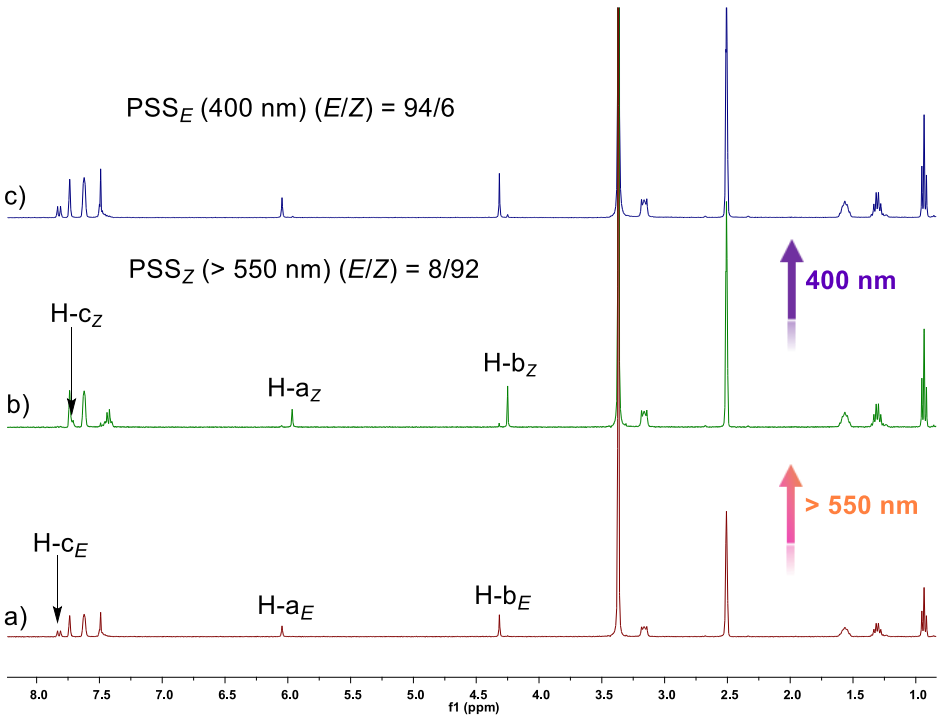

Fig. S18 ^{1}H NMR spectra (400 MHz, DMSO-d_6, 298K) for the solution of a) **XB-1**$_E$ (2.0 mM) and TBACl (2.0 mM), b) the PSS$_Z$ (> 550 nm) mixtures of **XB-1** (2.0 mM) and TBACl (2.0 mM), and c) the PSS$_E$ (400 nm) mixtures of **XB-1** (2.0 mM) and TBACl (2.0 mM).

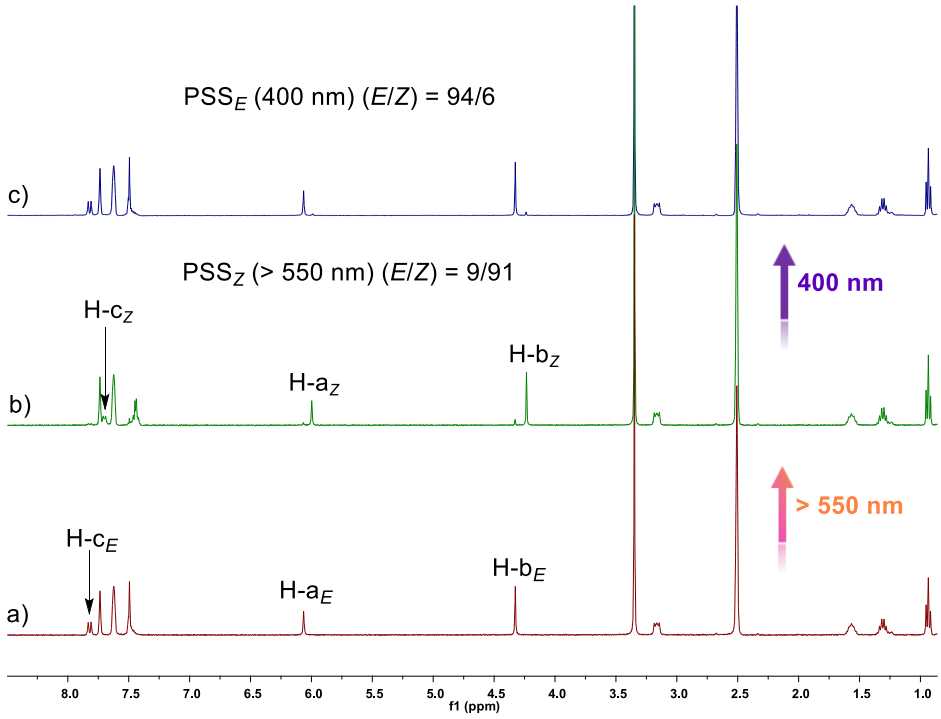

Fig. S19 ^{1}H NMR spectra (400 MHz, DMSO-d_6, 298K) for the solution of a) **XB-1**$_E$ (2.0 mM) and TBABr (2.0 mM), b) the PSS$_Z$ (> 550 nm) mixtures of **XB-1** (2.0 mM) and TBABr (2.0 mM), and c) the PSS$_E$ (400 nm) mixtures of **XB-1** (2.0 mM) and TBABr (2.0 mM).

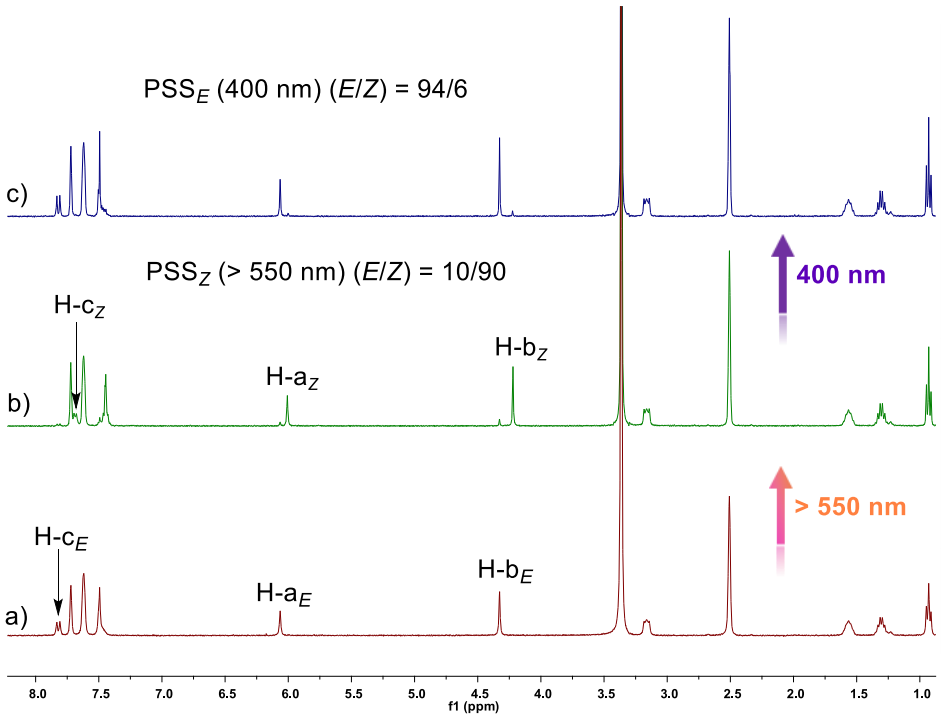

Fig. S20 ^{1}H NMR spectra (400 MHz, DMSO-d_6, 298K) for the solution of a) **XB-1**$_E$ (2.0 mM) and TBAI (2.0 mM), b) the PSS$_Z$ (> 550 nm) mixtures of **XB-1** (2.0 mM) and TBAI (2.0 mM), and c) the PSS$_E$ (400 nm) mixtures of **XB-1** (2.0 mM) and TBAI (2.0 mM).

Section 4: Photocontrolled anion abstraction mediated Friedel-Crafts reaction catalysed by XB-1

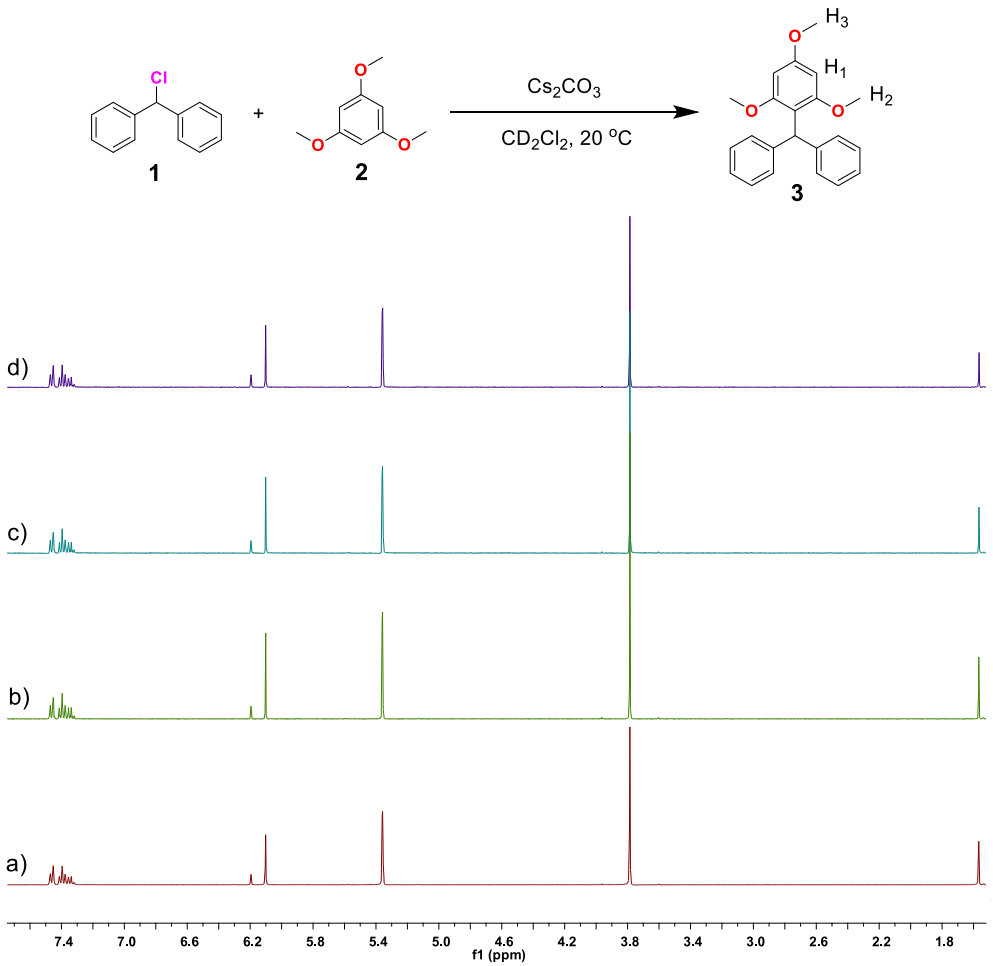

Fig. S21 Schematic representation of the benchmark reaction in the absence of catalyst in dark, and partial ^{1}H NMR (400 MHz, CD_2Cl_2, 298 K) spectra for the solution of reactants **1** (4.0 mM) and **2** (4.0 mM) in the presence of Cs_2CO_3 (4.0 mg / mL) after the rest of a) 5 min, b) 1 h, c) 2 h 10 min, and d) 96 h at 20 °C in dark. Note: no obvious proton signals (H_1 – H_3) of product **3** could be observed even after 96 hours.

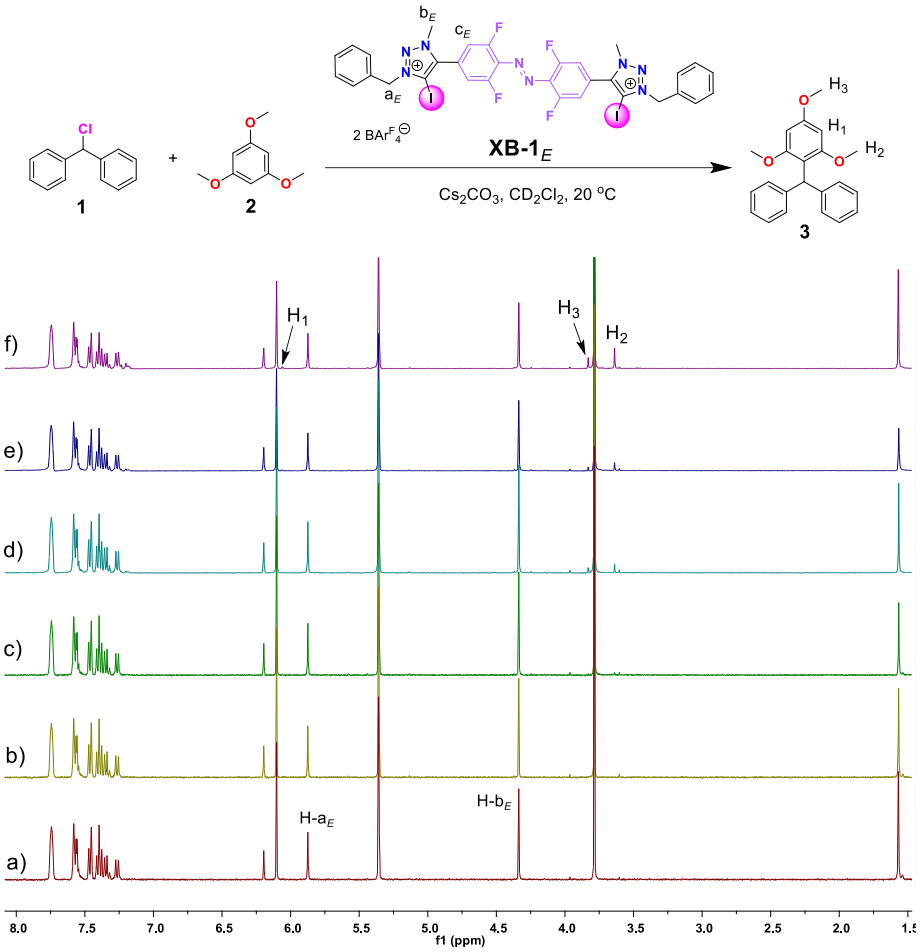

Fig. S22 Schematic representation of the benchmark reaction using **XB-1**$_E$ as catalyst, and partial ^{1}H NMR (400 MHz, CD_2Cl_2, 298 K) spectra for the solution of reactants **1** (4.0 mM), **2** (4.0 mM) and **XB-1**$_E$ (1.6 mM) in the presence of Cs_2CO_3 (4.0 mg / mL) after the rest of a) 5 min, b) 2 h 10 min, c) 6 h, d) 24 h, e) 31 h, and 96 h at 20 °C in dark.

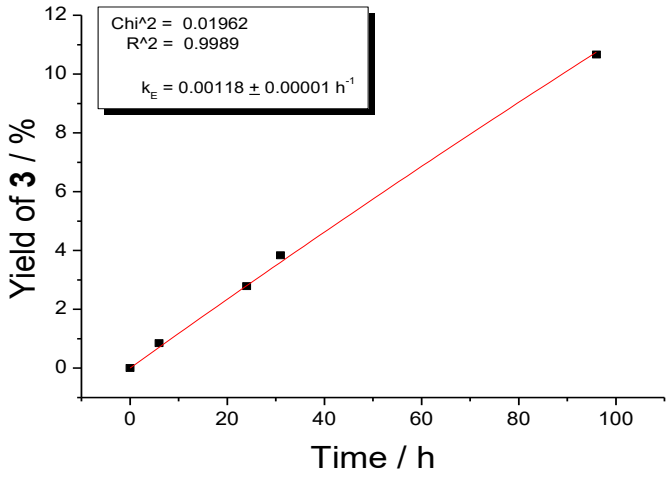

Fig. S23 Rate constants of Friedel-Crafts alkylation reaction between reactants **1** and **2** in the presence of **XB-1**$_E$.

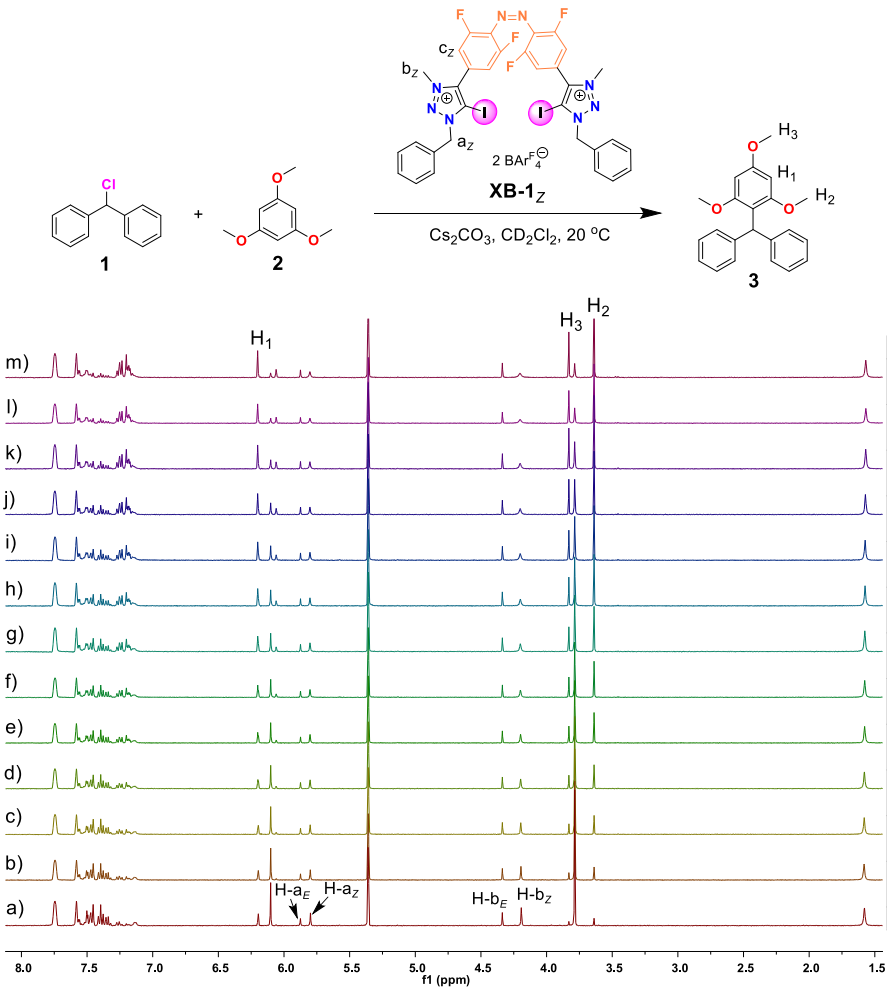

Fig. S24 Schematic representation of the benchmark reaction using **XB-1**$_Z$ as catalyst, and partial ^{1}H NMR (400 MHz, CD_2Cl_2, 298 K) spectra for the solution of reactants **1** (4.0 mM), **2** (4.0 mM) and PSS$_Z$ (> 550 nm) mixtures of **XB-1** (1.6 mM) in the presence of Cs_2CO_3 (4.0 mg / mL) after the rest of a) 4 min, b) 11 min, c) 17 min, d) 24 min, e) 31 min, f) 37 min, g) 44 min, h) 51 min, i) 57 min, j) 69 min, k) 85 min, l) 104 min, and m) 130 min at 20 °C in dark.

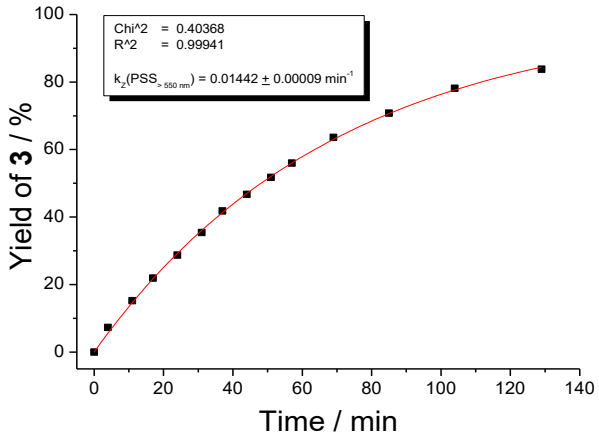

Fig. S25 Rate constants of Friedel-Crafts alkylation reaction between reactants **1** and **2** in the presence of PSS$_Z$ (> 550 nm) mixtures of **XB-1**.

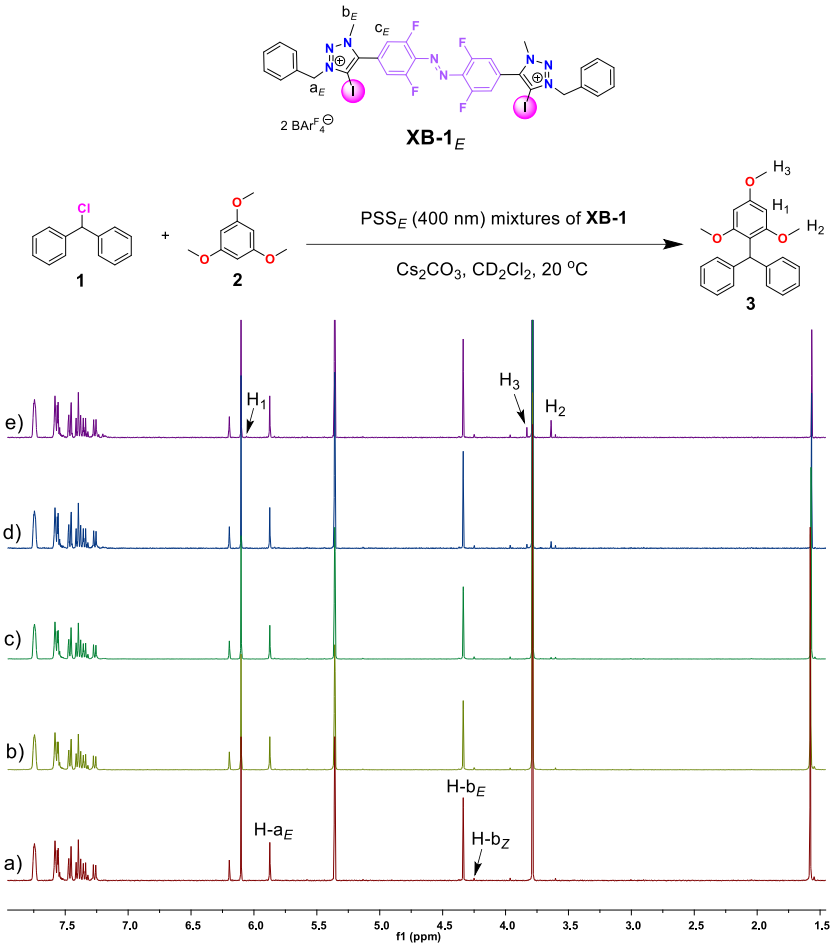

Fig. S26 Schematic representation of the benchmark reaction in the presence of PSS_E (400 nm) mixtures of **XB-1** as catalyst, and partial ^1H NMR (400 MHz, CD_2Cl_2, 298 K) spectra for the solution of reactants **1** (4.0 mM), **2** (4.0 mM) and PSS_E (400 nm) mixtures of **XB-1** (1.6 mM) in the presence of Cs_2CO_3 (4.0 mg / mL) after the rest of a) 5 min, b) 2 h, c) 6 h, d) 24 h, and e) 48 h at 20 °C in dark.

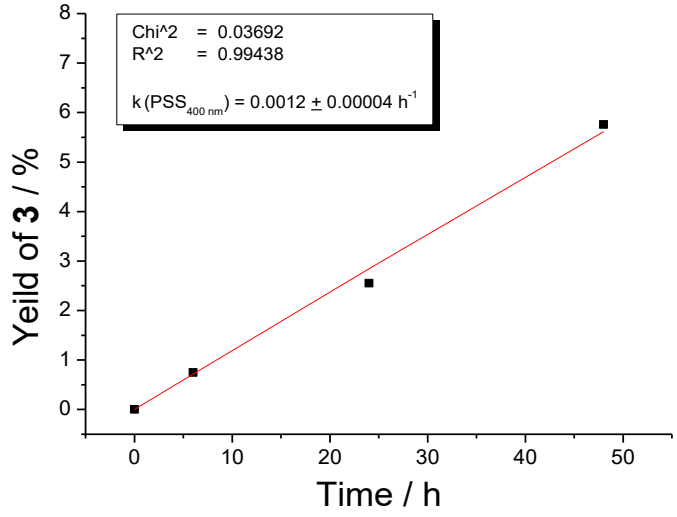

Fig. S27 Rate constants of Friedel-Crafts alkylation reaction between reactants **1** and **2** in the presence of PSS_E (400 nm) mixtures of **XB-1**.

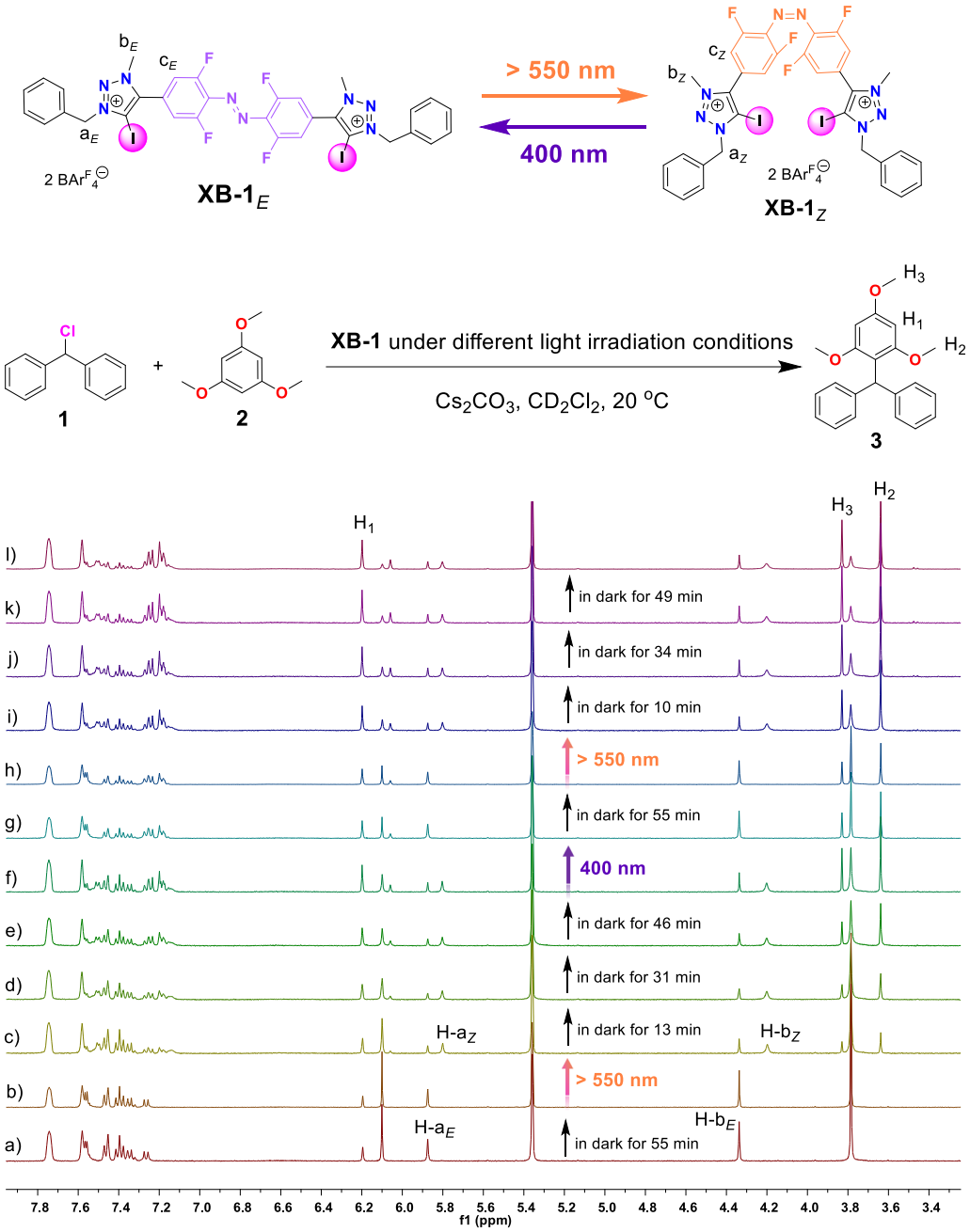

Fig. S28 Schematic representation for the yellow (>550 nm) / purple (400 nm) light induced *Z*/*E* photoisomerization of **XB-1** and catalyzed the benchmark reaction, and ^{1}H NMR (400 MHz, CD_2Cl_2, 298 K) spectra for the solution of reactants **1** (4.0 mM), **2** (4.0 mM) and **XB-1** (1.6 mM) in the presence of Cs_2CO_3 (4.0 mg / mL) under conditions of: a) as prepared pristine reaction solution; b) after rest for 55 min in dark; c) after exposing to yellow (>550 nm) light irradiation for 10 min; d) after removing the yellow (>550 nm) light source and rest in dark for 13 min; e) rest in dark for 31 min; f) rest in dark for 46 min; g) after exposing the $PSS_{>550nm}$ mixtures to purple (400 nm) light irradiation for 15 seconds; h) after removing the purple (400 nm) light source and rest in dark for 55 min; i) after exposing the PSS_{400nm} mixtures to yellow (>550 nm) light irradiation for 10 min; j) after removing the yellow (>550 nm) light source and rest in dark for 10 min, k) rest in dark for 34 min; and l) rest in dark for 49 min.

Section 5: Photocontrolled cationic polymerization catalyzed by XB-1

The procedure of polymerization in the absence of catalyst: To a solution of compound **1** (0.4 mg, 2.0 μmol, 1.0 eq.) in CD_2Cl_2 (0.5 mL) was added monomer *p*-methylphenylene (**pMeS**) (11.8 mg, 100 μmol, 50 eq.), the mixture was rest for different time intervals, the corresponding ^1H NMR spectrum of which was then recorded and displayed in Fig.S29.

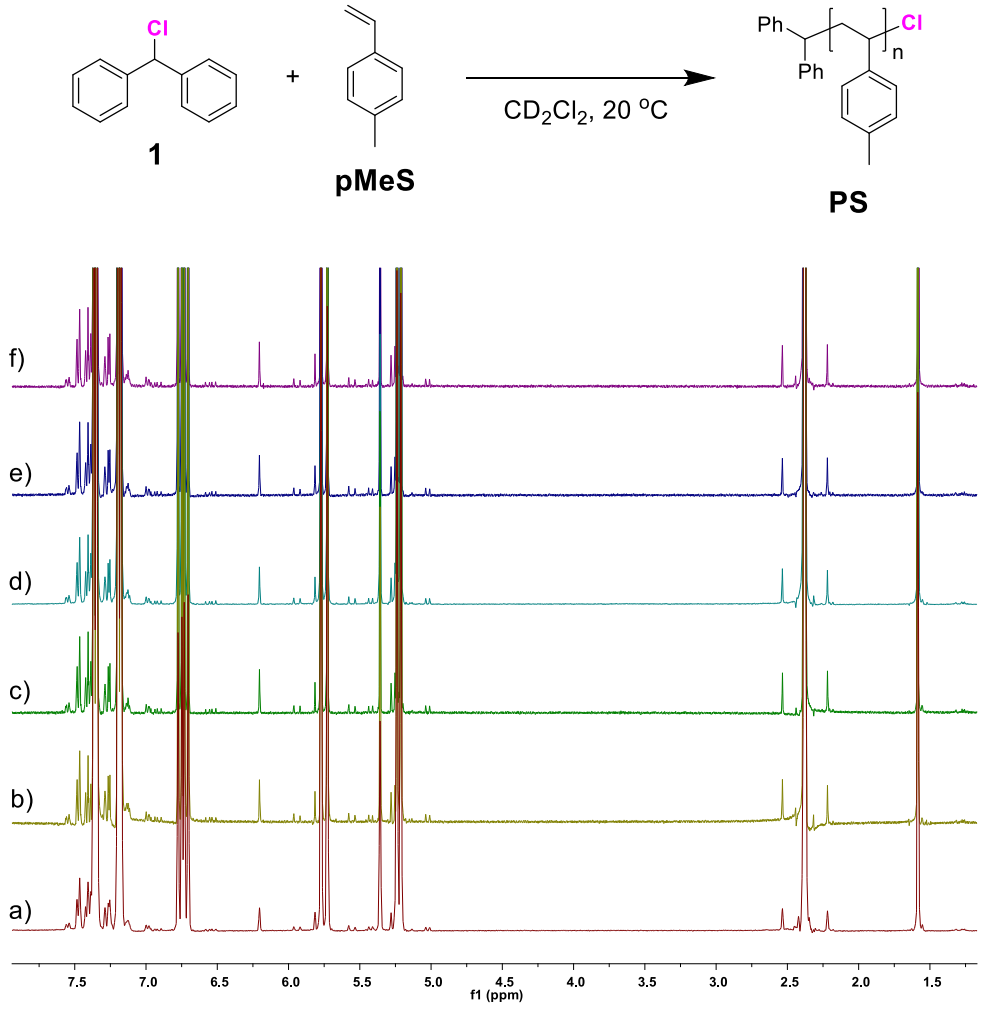

Fig. S29 Schematic representation for the cationic polymerization of **pMeS** in the absence of catalyst, and partial ^1H NMR (400 MHz, CD_2Cl_2, 298 K) spectra for the solution of initiator **1** (4.0 mM) and **pMeS** (200 mM) after the rest for a) 10 min, b) 1 h, c) 2 h, d) 8 h, e) 31 h and f) 48 h at 20 °C.

The procedure for the cationic polymerization of pMeS in the presence of XB-1$_E$ as catalyst: The catalyst **XB-1**$_E$ (2.1 mg, 0.8 μmol, 0.4 eq.) and monomer **pMeS** (11.8 mg, 100 μmol, 50 eq.) was dissolved in CD_2Cl_2 (0.5 mL), to the solution of which was further added compound **1** (0.4 mg, 2.0 μmol, 1.0 eq.), the resulting mixture was then rest for different time intervals, the corresponding ^{1}H NMR spectrum was recorded and displayed in Fig.S30.

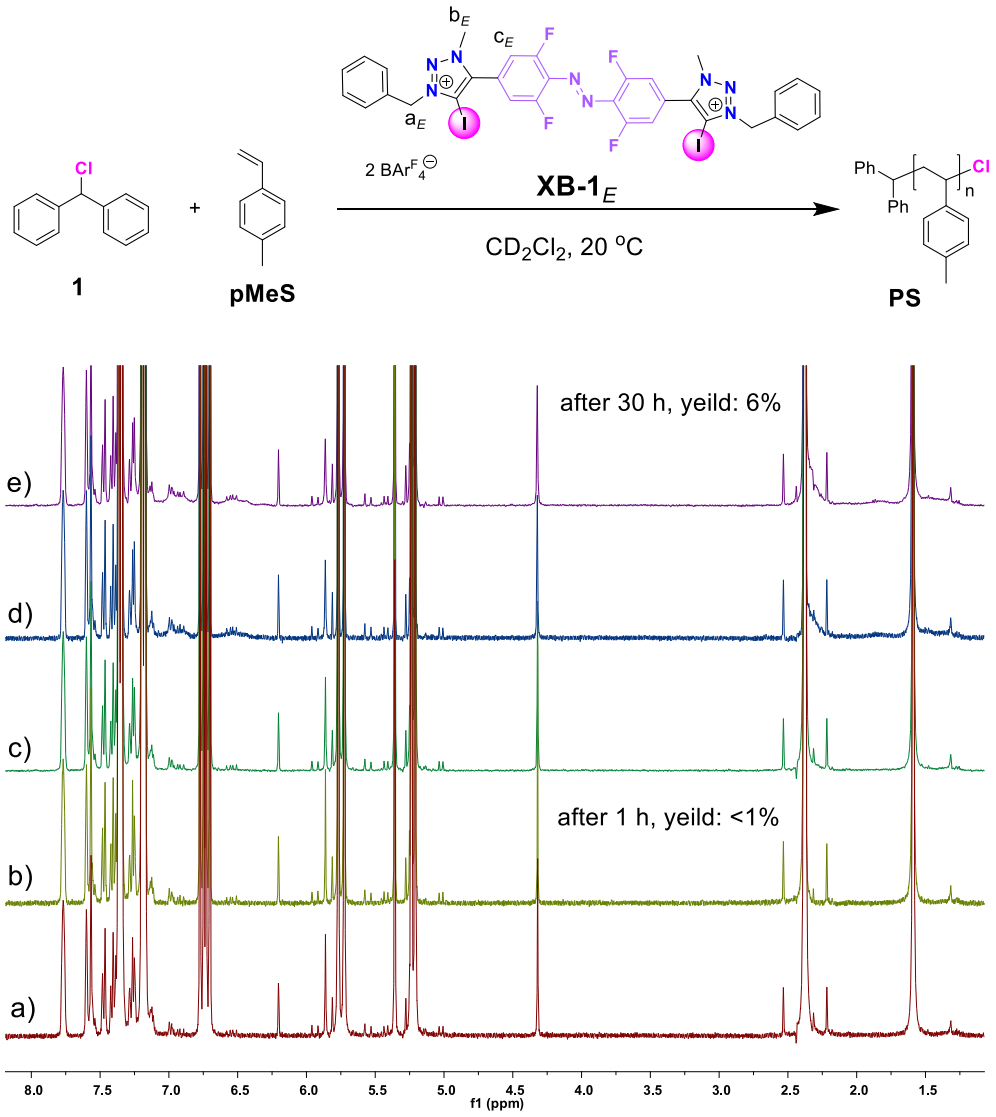

Fig. S30 Schematic representation for the cationic polymerization of **pMeS** in the presence of pristine **XB-1**$_E$ as catalyst, and partial ^{1}H NMR (400 MHz, CD_2Cl_2, 298 K) spectra for the solution of initiator **1** (4.0 mM) and **pMeS** (200 mM) after the rest for a) 5 min, b) 1 h, c) 6.5 h, d) 24 h and e) 30 h at 20 °C.

The procedure for the cationic polymerization of pMeS in the presence of PSS$_Z$ (>550 nm) mixtures of XB-1 as catalyst: The catalyst **XB-1**$_E$ (2.1 mg, 0.8 μmol, 0.4 eq.) and monomer **pMeS** (11.8 mg, 100 μmol, 50 eq.) was dissolved in CD_2Cl_2 (0.5 mL), the mixture solution was exposed to yellow (>550 nm) light irradiation for 30 min. Then, compound **1** (0.4 mg, 2.0 μmol, 1.0 eq.) was added, and the resulting mixture was rest for different time intervals, the corresponding ^{1}H NMR spectrum was recorded and displayed in Fig.S31.

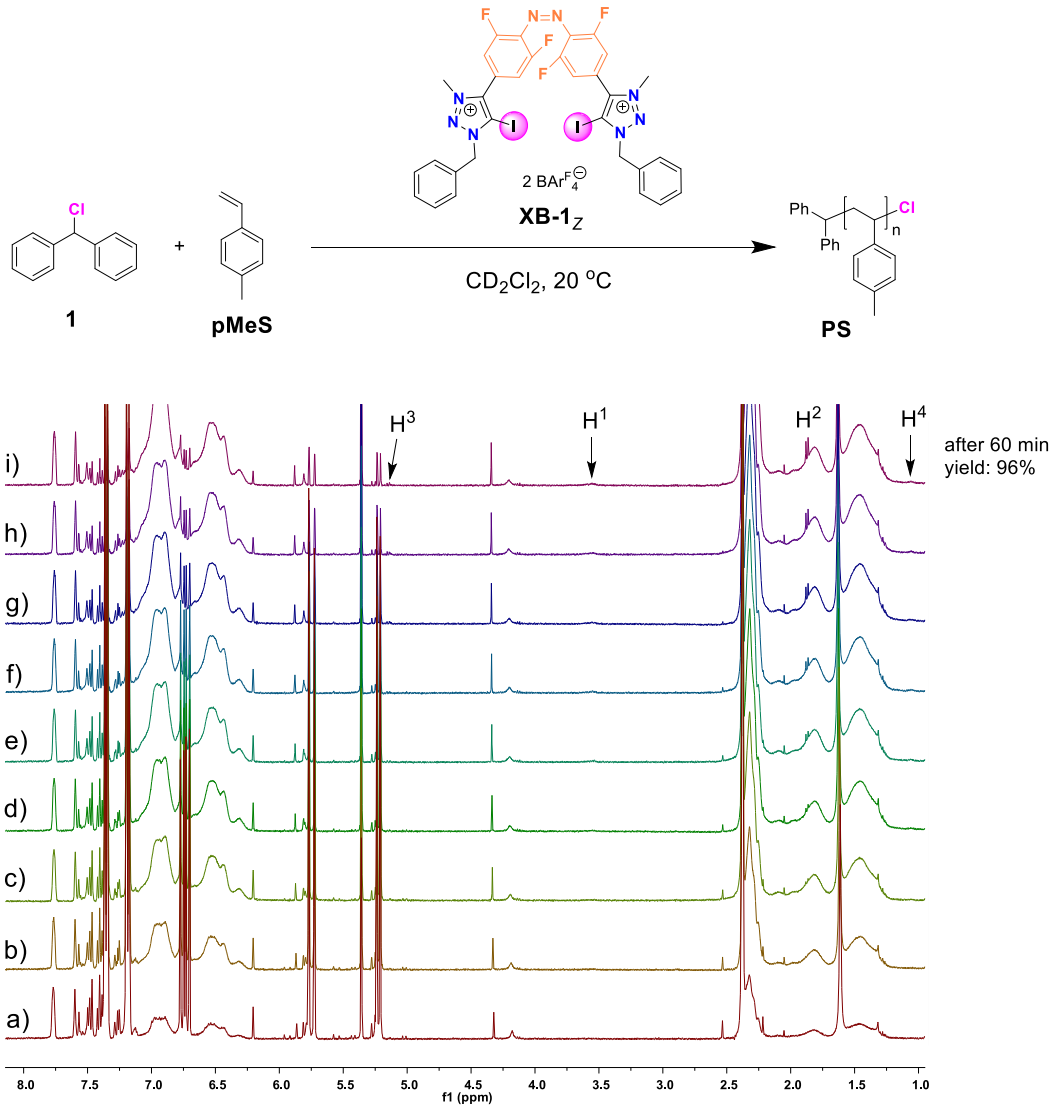

Fig. S31 Schematic representation for the cationic polymerization of **pMeS** in the presence of PSS$_Z$ (> 550 nm) mixtures of **XB-1** as catalyst, and partial ^{1}H NMR (400 MHz, CD_2Cl_2, 298 K) spectra for the solution of initiator **1** (4.0 mM) and **pMeS** (200 mM) and PSS$_Z$ (> 550 nm) mixtures of **XB-1** (1.6 mM) after the rest for a) 6 min, b) 10 min, c) 15 min, d) 20 min, e) 25 min, f) 30 min, g) 40 min, h) 50 min and i) 60 min at 20 °C. Not: for the assignment of the marked protons, please see Scheme S2.

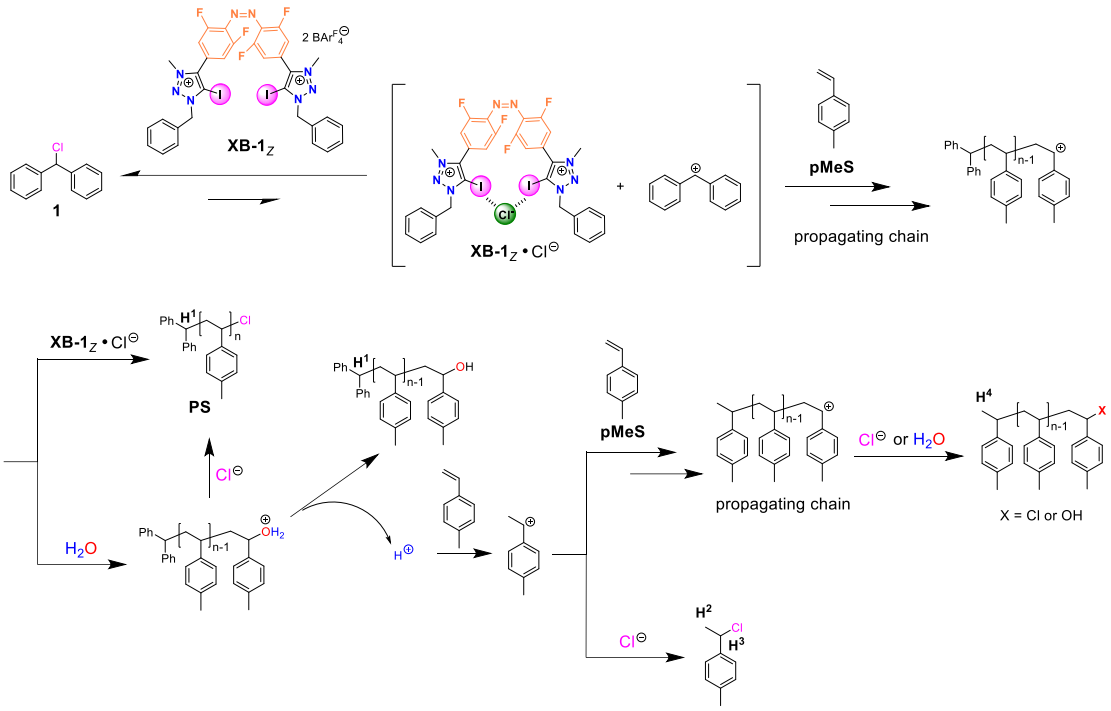

Scheme S2. Schematic representation for the **XB-1**$_Z$ catalyzed cationic polymerization of **pMeS** and the possible chain transfer reaction pathways.

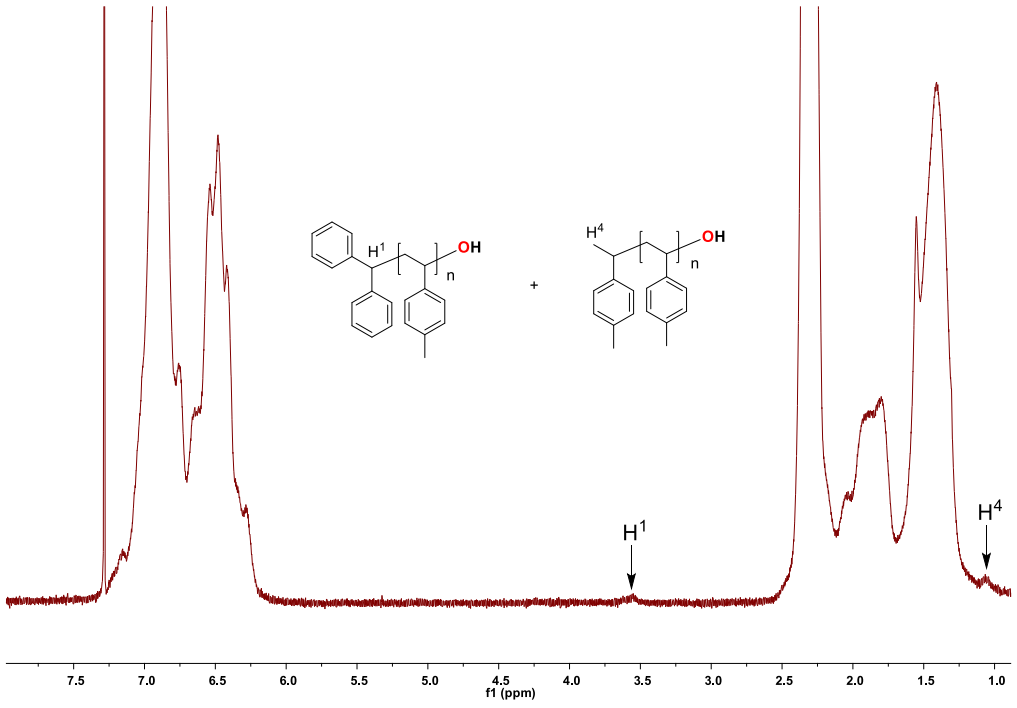

Fig. S32 The ^{1}H NMR (400 MHz, CD_2Cl_2, 298 K) spectrum of the polymer product after the polymerization for 60 min was quenched by the addition of 2M NH_3 solution in methanol (4 mL)[4]. Polymerization conditions: monomer **pMeS** (200 mM, 50 eq.), compound **1** (4.0 mM, 1.0 eq.), and PSS$_Z$ (>550 nm) mixtures of **XB-1** (1.6 mM, 0.4 eq.) in CD_2Cl_2 at 20 °C.

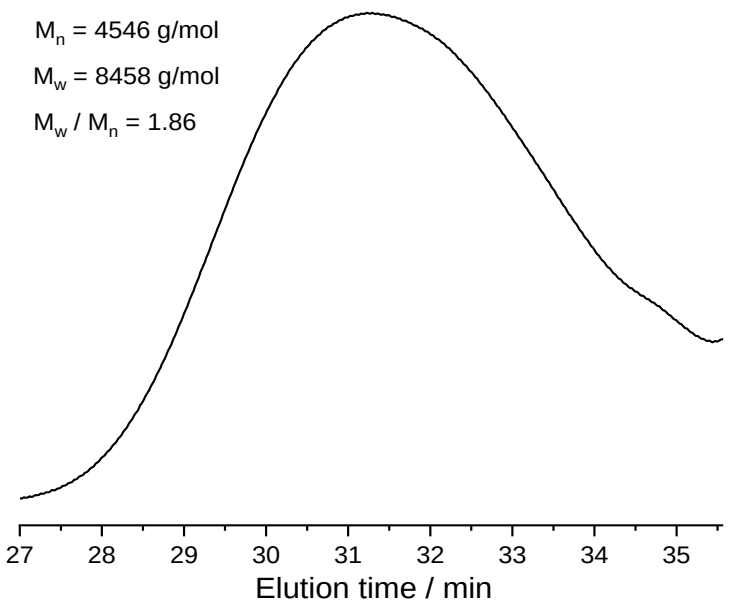

Fig. S33 The GPC trace of polymer product after the polymerization for 60 min was quenched by the addition of 2M NH_3 solution in methanol (4 mL)[4]. Polymerization conditions: monomer **pMeS** (200 mM, 50 eq.), compound **1** (4.0 mM, 1.0 eq.), and PSS_Z (>550 nm) mixture of **XB-1** 1.6 mM, 0.4 eq.) in CD_2Cl_2 at 20 °C.

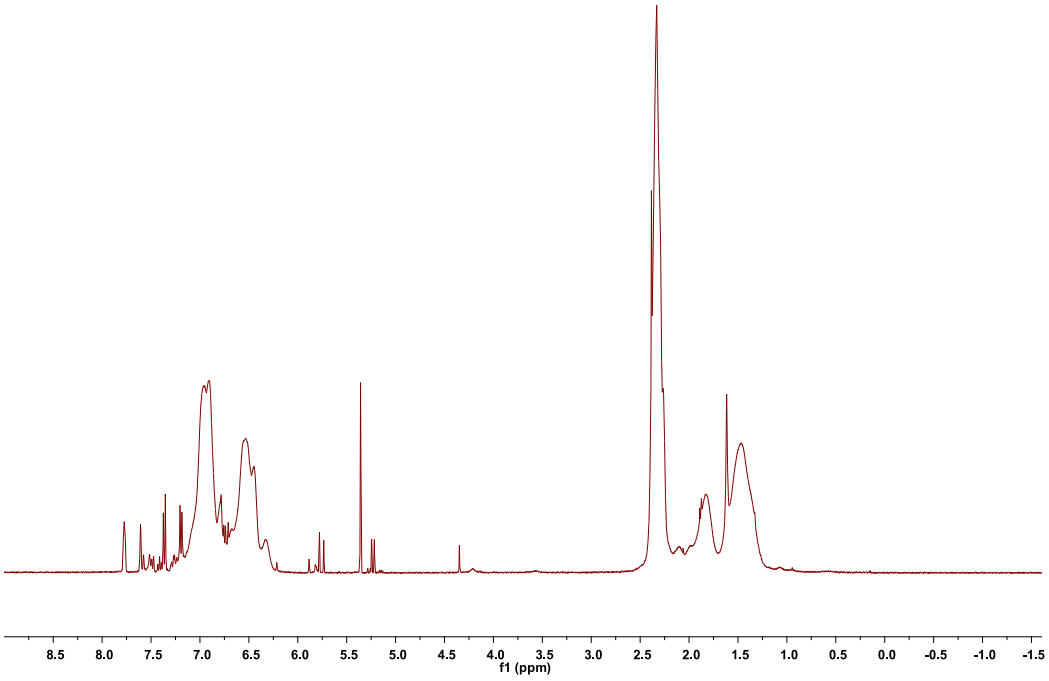

Fig. S34 The ^1H NMR (400 MHz, CD_2Cl_2, 298 K) spectra for the solution of initiator **1** (4.0 mM) and **pMeS** (400 mM) and PSS_Z (> 550 nm) mixtures of **XB-1** (1.6 mM) after the rest for 60 min at 20 °C.

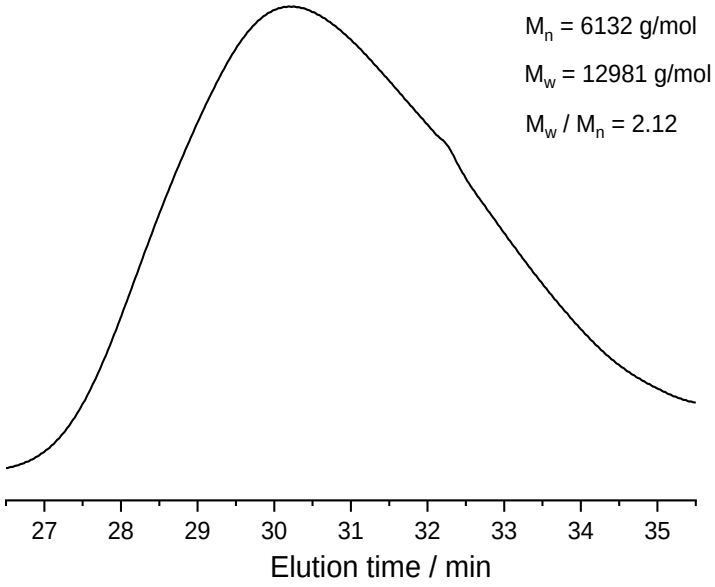

Fig. S35 The GPC trace of polymer product after the polymerization for 60 min was quenched by the addition of 2M NH_3 solution in methanol (4 mL)[4]. Polymerization conditions: PSS_Z (>550 nm) mixtures of **XB-1** (1.6 mM, 0.4 eq.), monomer **pMeS** (400 mM, 100 eq.) and compound **1** (4.0 mM, 1.0 eq.) in CD_2Cl_2 at 20 °C.

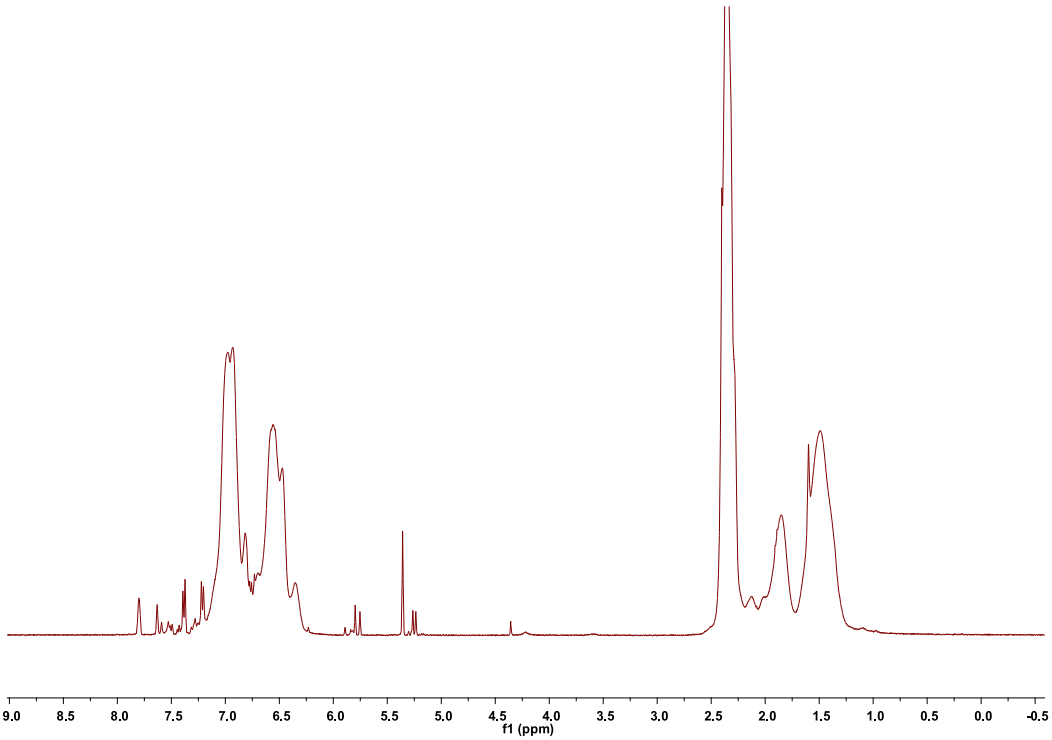

Fig. S36 The ^1H NMR (400 MHz, CD_2Cl_2, 298 K) spectra for the solution of initiator **1** (4.0 mM) and **pMeS** (800 mM) and PSS_Z (> 550 nm) mixtures of **XB-1** (1.6 mM) after the rest for 60 min at 20 °C.

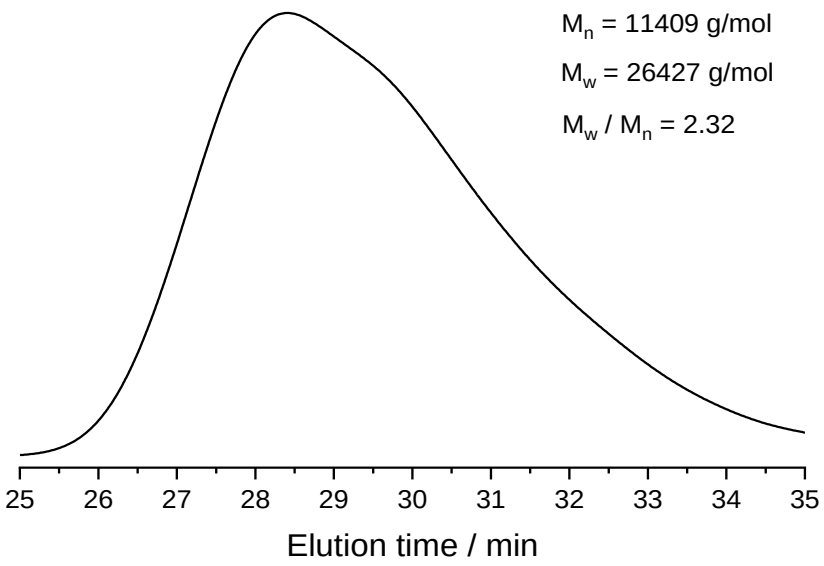

Fig. S37 The GPC trace of polymer product after the polymerization for 60 minwas quenched by the addition of 2M NH_3 solution in methanol (4 mL)[4]. Polymerization conditions: PSS_Z (> 550 nm) mixture of **XB-1** (1.6 mM, 0.4 eq.), monomer **pMeS** (800 mM, 200 eq.) and compound **1** (4.0 mM, 1.0 eq.) in CD_2Cl_2 at 20 ºC.

The procedure of the photoswitchable catalysis of the cationic polymerization: To a solution of compound **1** (0.4 mg, 2.0 μmol, 1.0 eq.) in CD_2Cl_2 (0.5 mL) was added monomer **pMeS** (11.8 mg, 100 μmol, 50 eq.), followed by the addition of the catalyst **XB-1**$_E$ (2.1 mg, 0.8 μmol, 0.4 eq.). The resulting mixture was first rest in dark for 10 min, and the ^{1}H NMR spectrum of the solution was recorded. Then, the sample solution was subjected to yellow (>550 nm) light irradiation for 10 min, followed by recording the ^{1}H NMR spectrum of the PSS_Z (>550 nm) mixture solution. The yellow (>550 nm) light irradiated sample was further exposed to purple (400 nm) light irradiation for 15 seconds, followed by recording the ^{1}H NMR spectrum of the PSS_E (400 nm) mixture solution. The purple (400 nm) light irradiated mixture solution was then rest in dark for 10 min, after which the sample was subjected to the second round yellow (>550 nm) light irradiation, and the followed operation procedures were similar to the first round. The corresponding ^{1}H NMR spectra recorded during the above repetitive light irradiation experiments were displayed in Fig.S38.

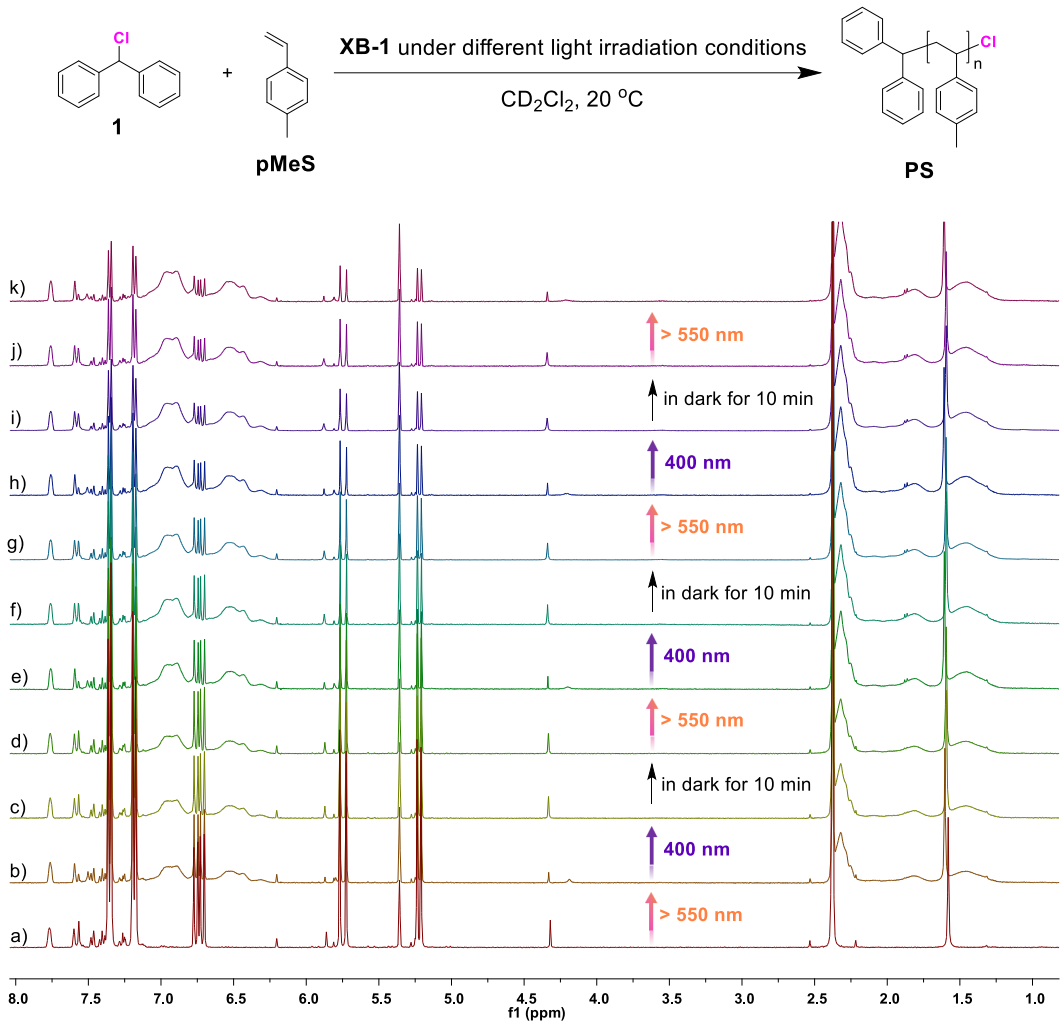

Fig. S38 Schematic representation for the photocontrolled cationic polymerization catalyzed by the PSS_Z (>550 nm) / PSS_E (400 nm) mixture of **XB-1**, and partial ^1H NMR (400 MHz, CD_2Cl_2, 298 K) spectra for the mixture solution of compound **1** (4.0 mM, 1.0 eq.), **XB-1** (1.6 mM, 0.4 eq.) and **pMeS** (200 mM, 50 eq.) under conditions of: a) as prepared mixture solution after rest in dark for 10 min; b) after yellow (>550 nm) light irradiation for 10 min; c) after the PSS_Z (>550nm) mixture was exposed to purple (400 nm) light irradiation for 15 seconds; d) after the PSS_E (400nm) mixture was rest in dark for 10 min; e) after the second round yellow (>550 nm) light irradiation for 10 min; f) after the PSS_Z (>550nm) mixture was exposed to second round purple (400 nm) light irradiation for 15 seconds; g) after the PSS_E (400nm) mixture was rest in dark for 10 min; h) after the third round yellow (>550 nm) light irradiation for 10 min; i) after the PSS_Z (>550nm) mixture was exposed to third round purple (400 nm) light irradiation for 15 seconds; j) after the PSS_E (400nm) mixture was rest in dark for 10 min; k) after the fourth round yellow (>550 nm) light irradiation for 10 min.

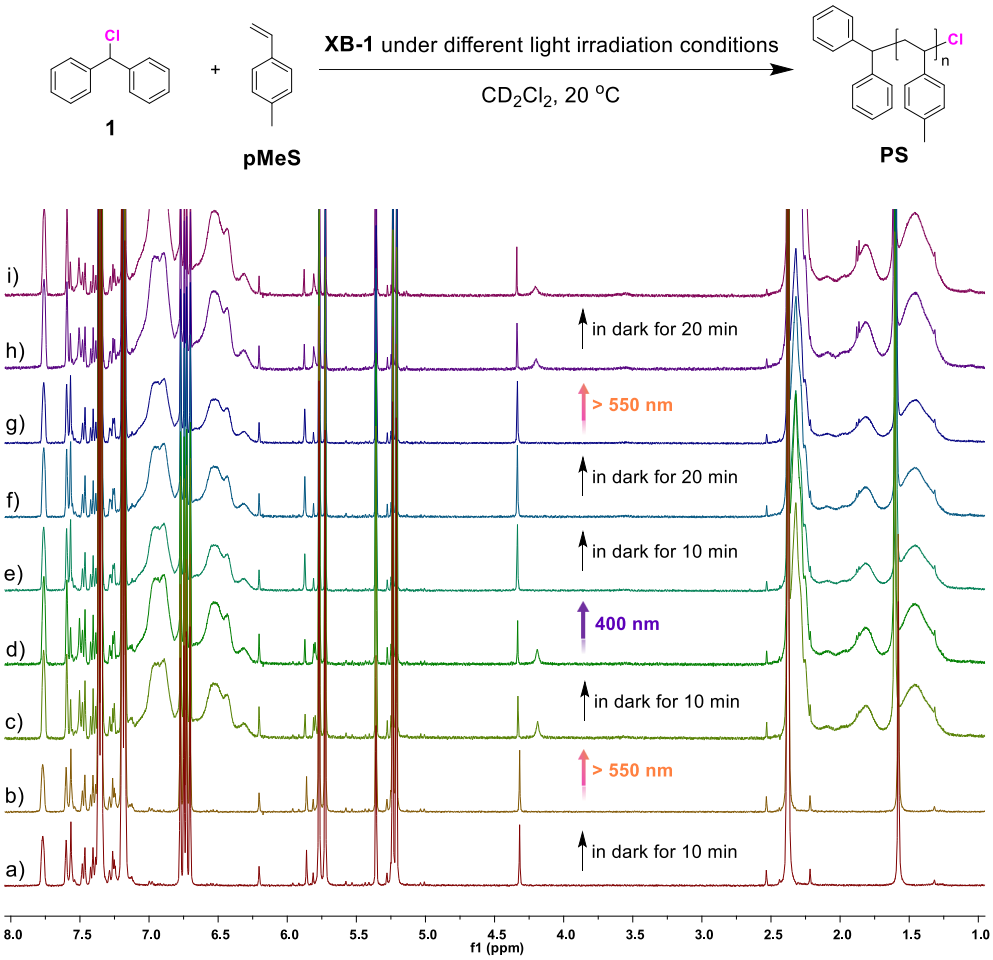

Fig. S39 Schematic representation for the photocontrolled cationic polymerization catalyzed by the PSS_Z (>550 nm) / PSS_E (400 nm) mixture of **XB-1**, and ^{1}H NMR (400 MHz, CD_2Cl_2, 298 K) spectra for the mixture solution of compound **1** (4.0 mM, 1.0 eq.), **XB-1** (1.6 mM, 0.4 eq.) and **pMeS** (200 mM, 50 eq.) under conditions: a) as prepared mixture solution after rest for 10 min and b) 20 min; c) after yellow (>550 nm) light irradiation for 10 min; d) after removing the yellow (>550 nm) light source and rest in dark for 10 min; e) after the PSS_Z (>550nm) mixture was exposed to purple (400 nm) light irradiation for 15 seconds; after removing the purple (400 nm) light source and rest in dark for f) 10 min, g) 20 min; h) after exposing the PSS_E (400nm) mixtures to yellow (>550 nm) light irradiation for 10 min; i) after removing the yellow (>550 nm) light source and rest in dark for 20 min.

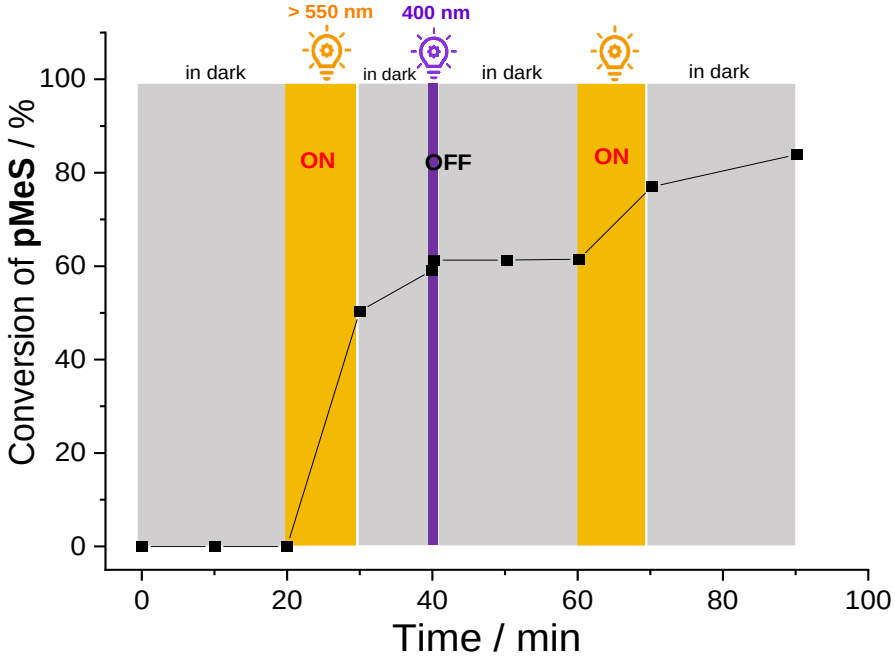

Fig. S40 Photoswitchable control of the XB-based catalysis on the cationic polymerization of **pMeS** with intermittent yellow (>550 nm, ON state) and purple (400 nm, OFF state) light irradiation. Note: the conversion changes of **pMeS** *versus* time were obtained based on the recorded ^{1}H NMR spectra in Fig.S39.

Section 6: The ^{1}H NMR, ^{13}C NMR, ^{19}F NMR and MS spectra for new compounds

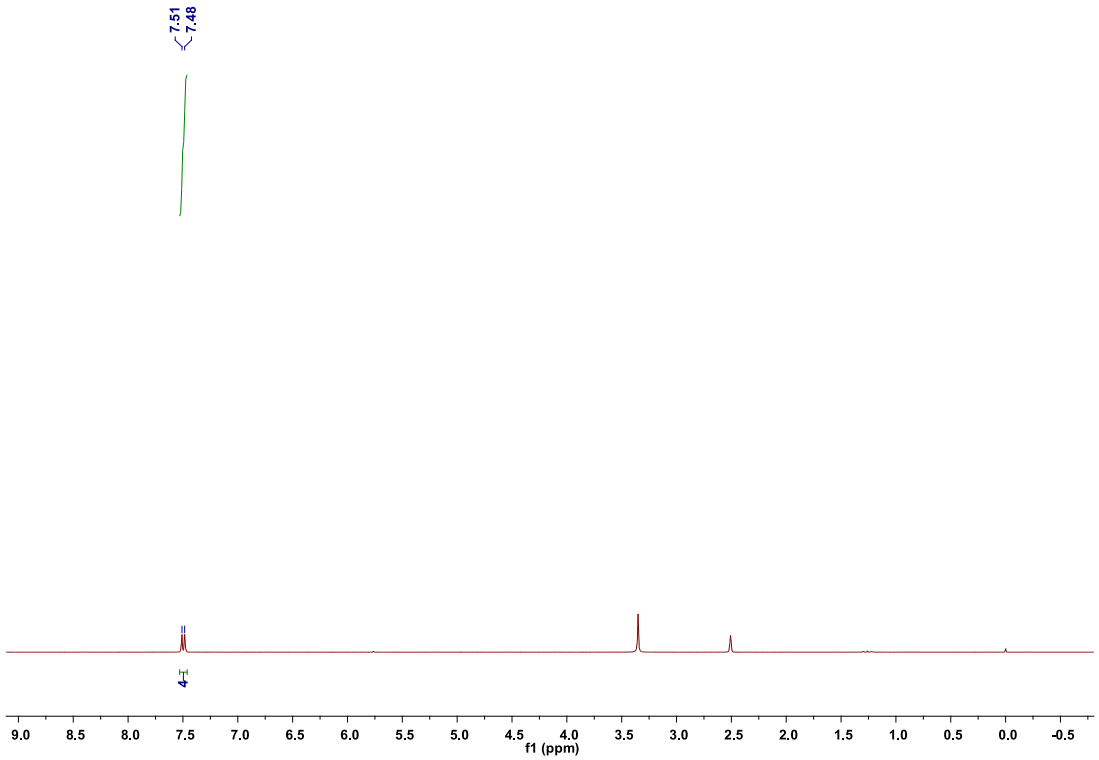

^{1}H NMR spectrum (400 MHz, DMSO-d_6, 298 K) of compound **5**.

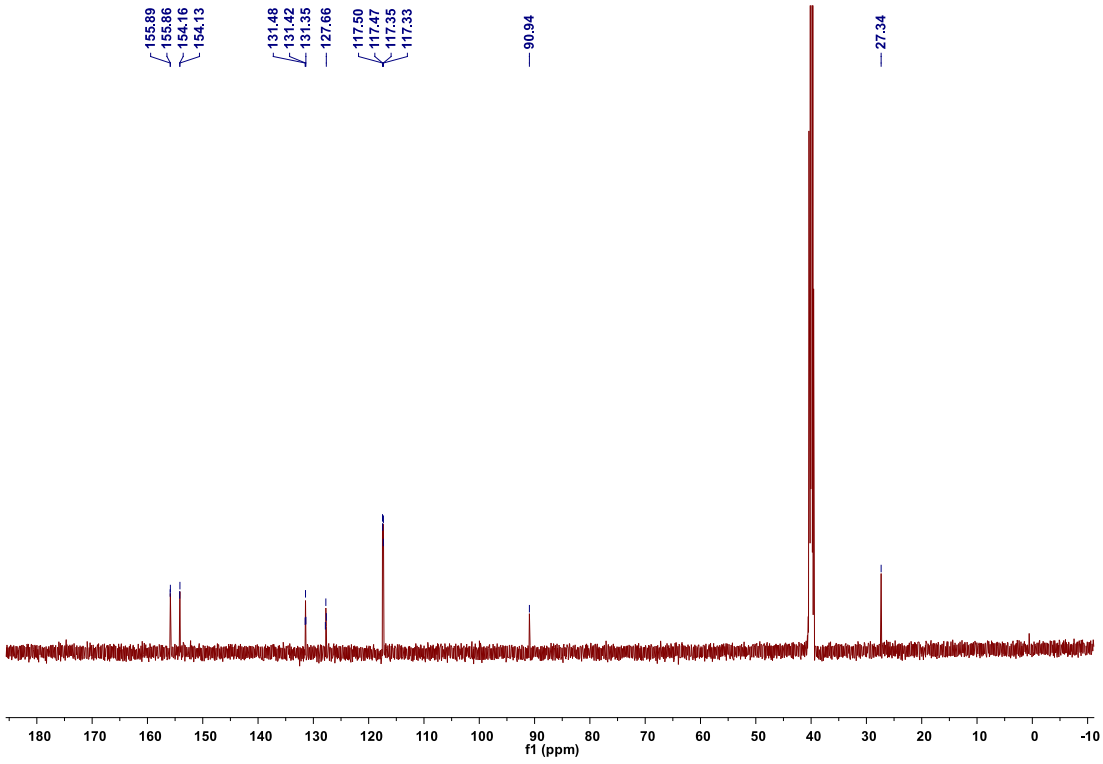

^{13}C NMR spectrum (150 MHz, DMSO-d_6, 298 K) of compound **5**.

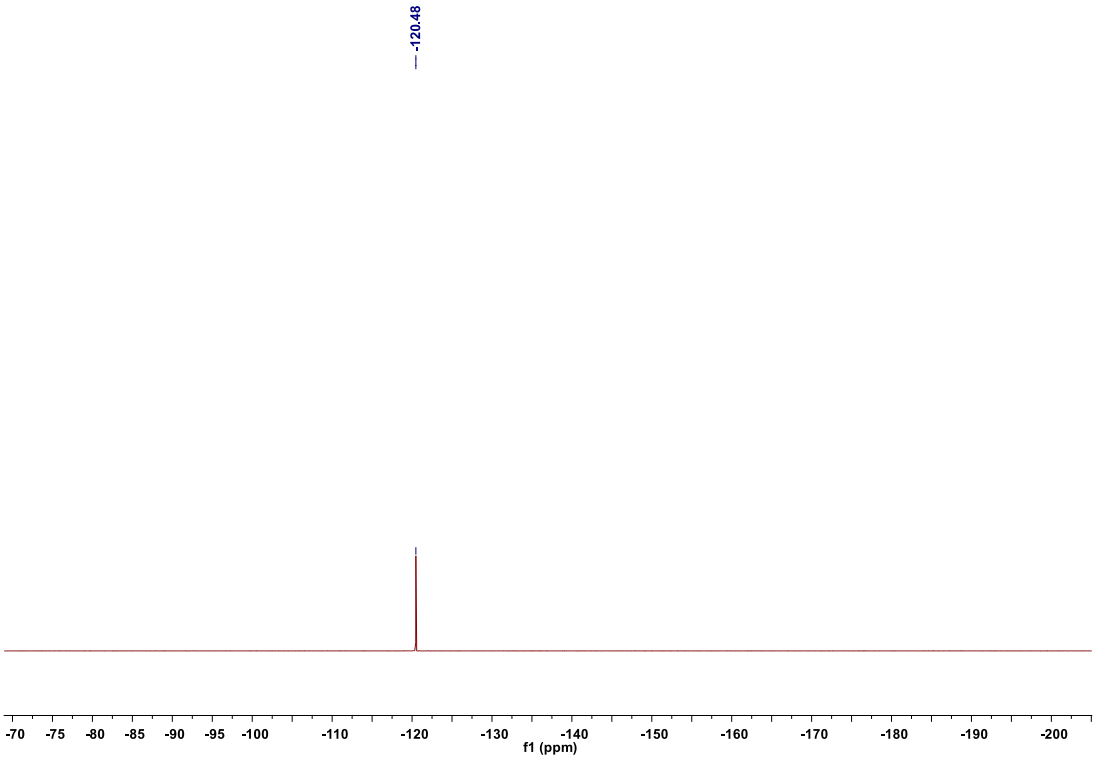

^{19}F NMR spectrum (376 MHz, DMSO-d_6, 298 K) of compound **5**.

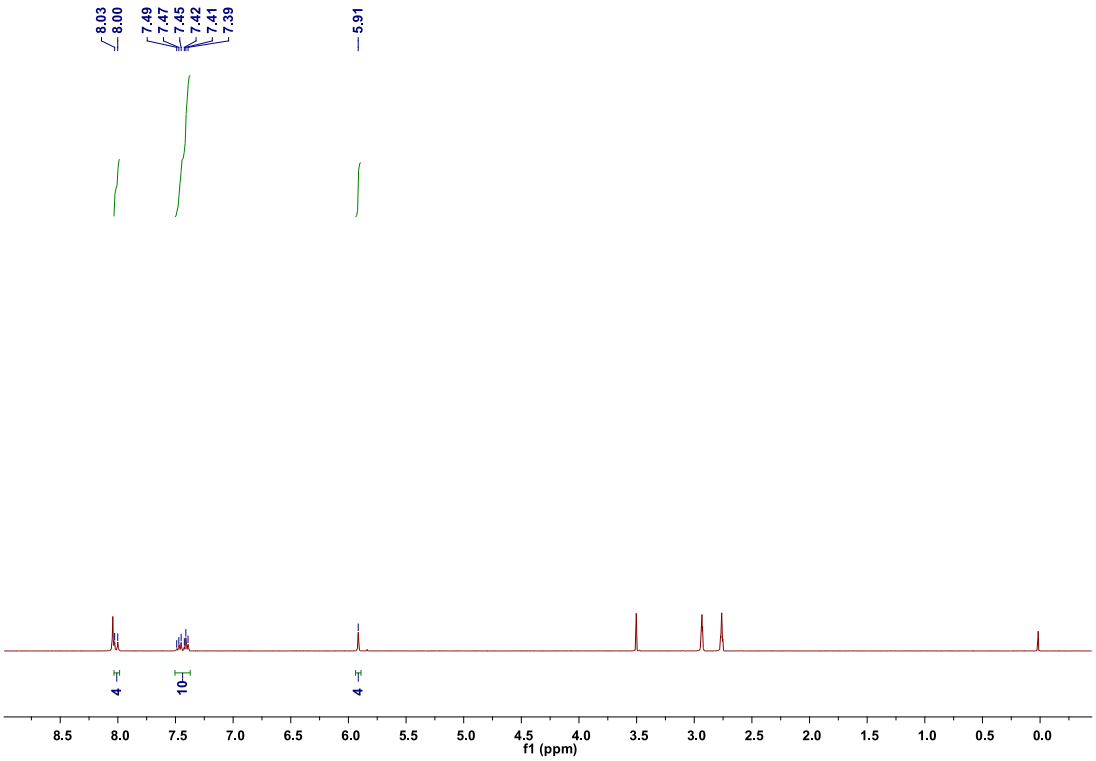

^{1}H NMR spectrum (400 MHz, DMF-d_7, 298 K) of compound **7**.

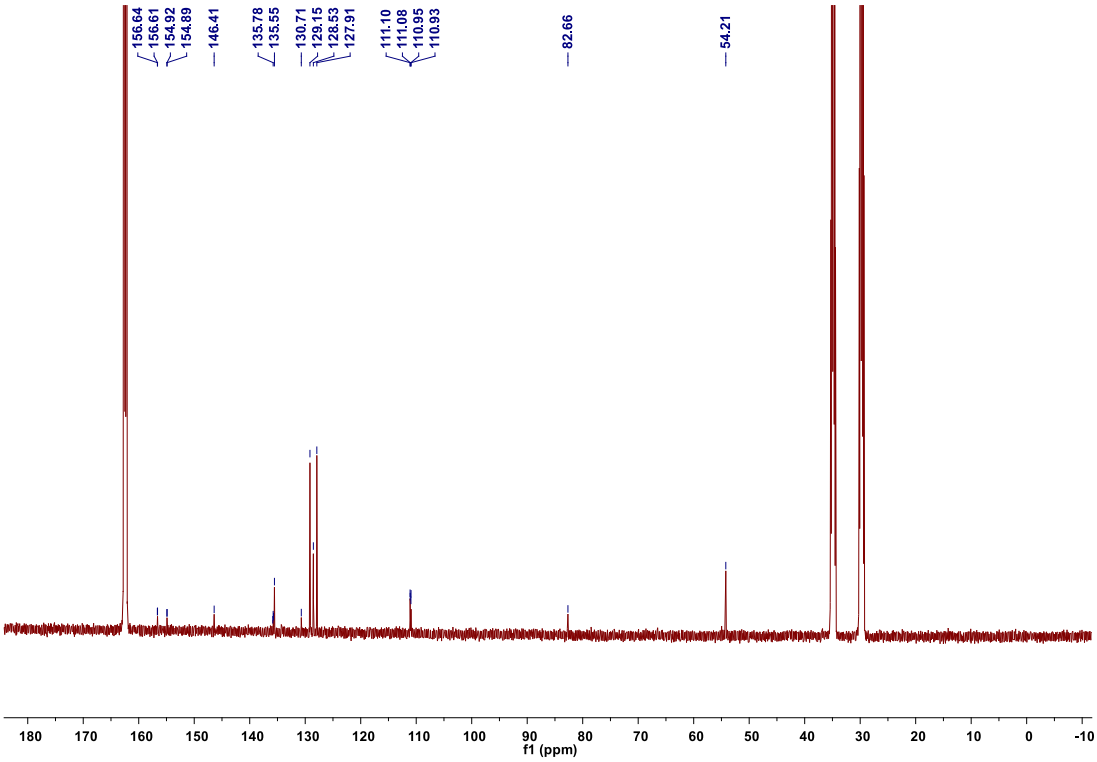

^{13}C NMR spectrum (150 MHz, DMF-d_7, 298 K) of compound **7**.

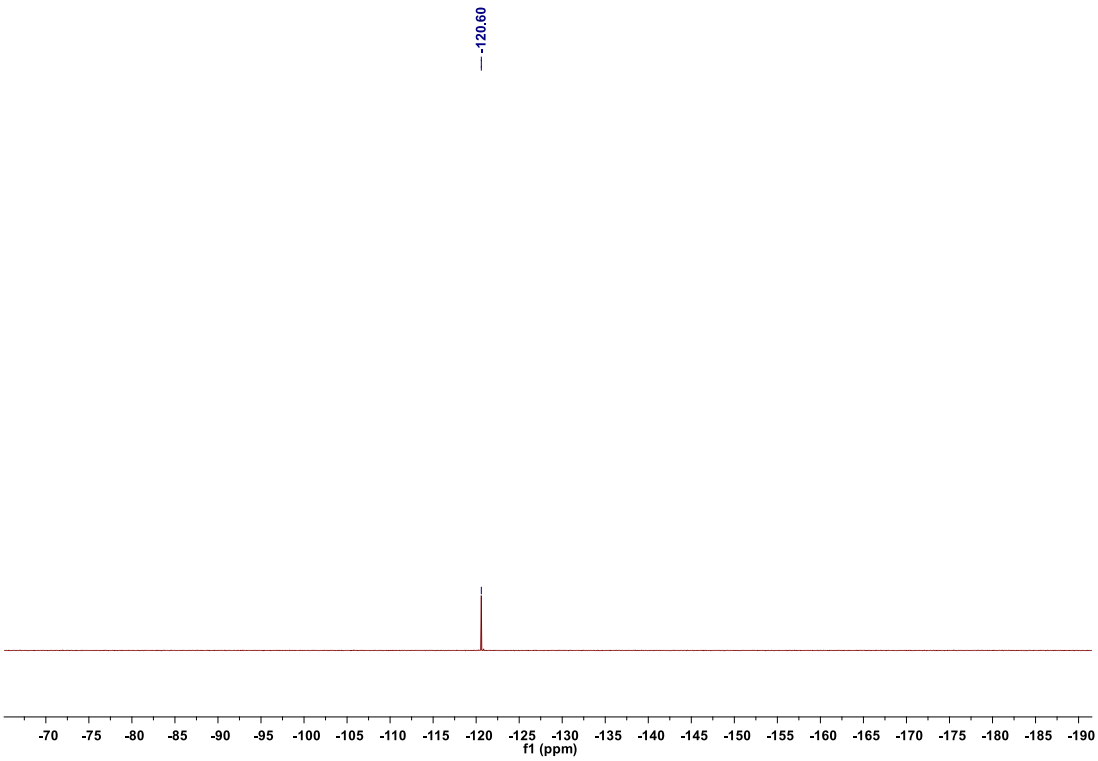

^{19}F NMR spectrum (376 MHz, DMF-d_7, 298 K) of compound **7**.

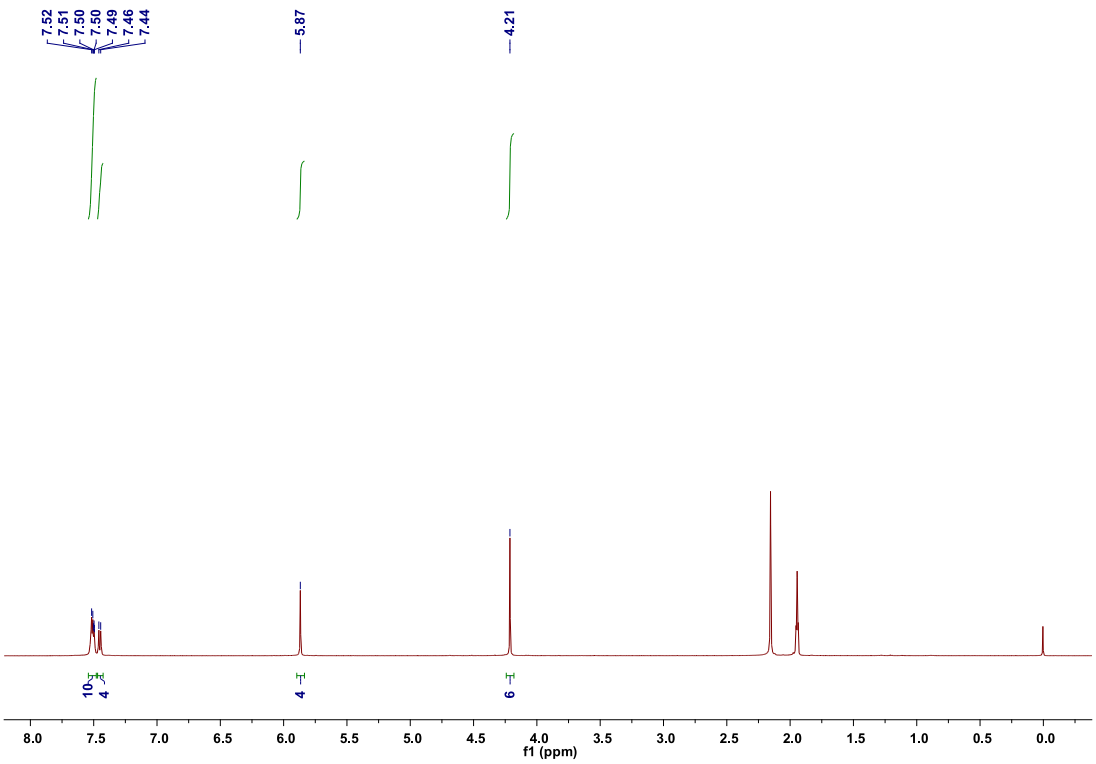

^{1}H NMR spectrum (600 MHz, CD_3CN, 298 K) of compound **8**.

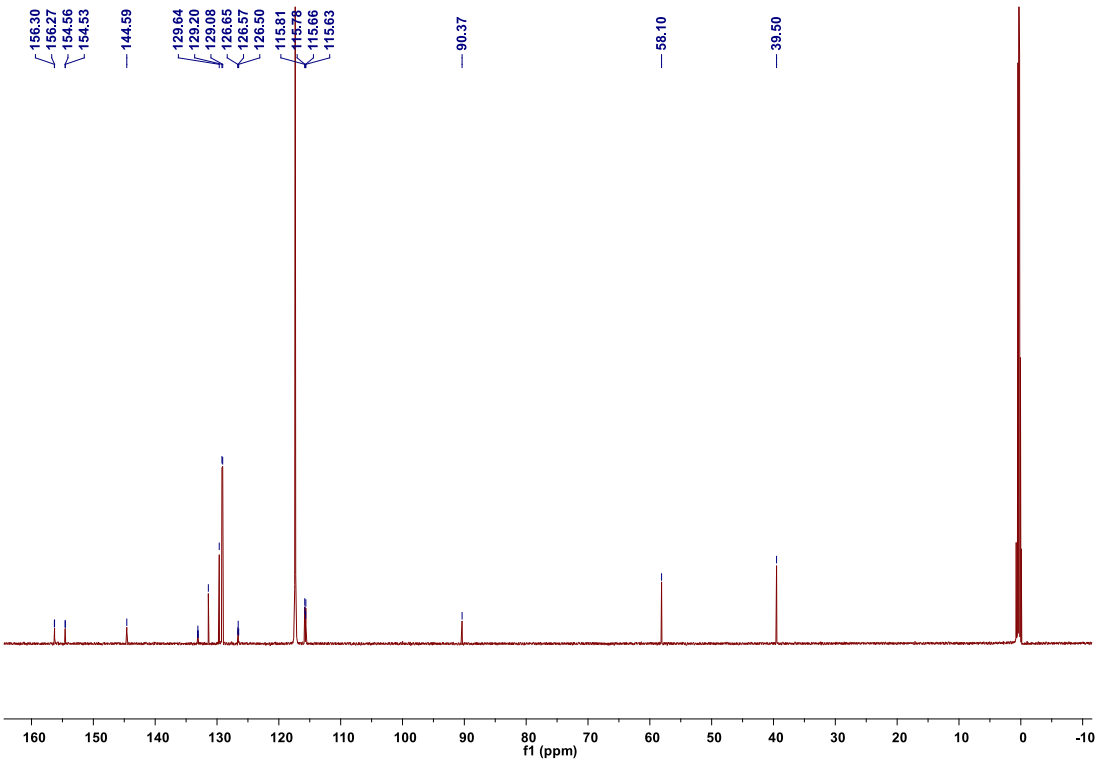

^{13}C NMR spectrum (150 MHz, CD_3CN, 298 K) of compound **8**.

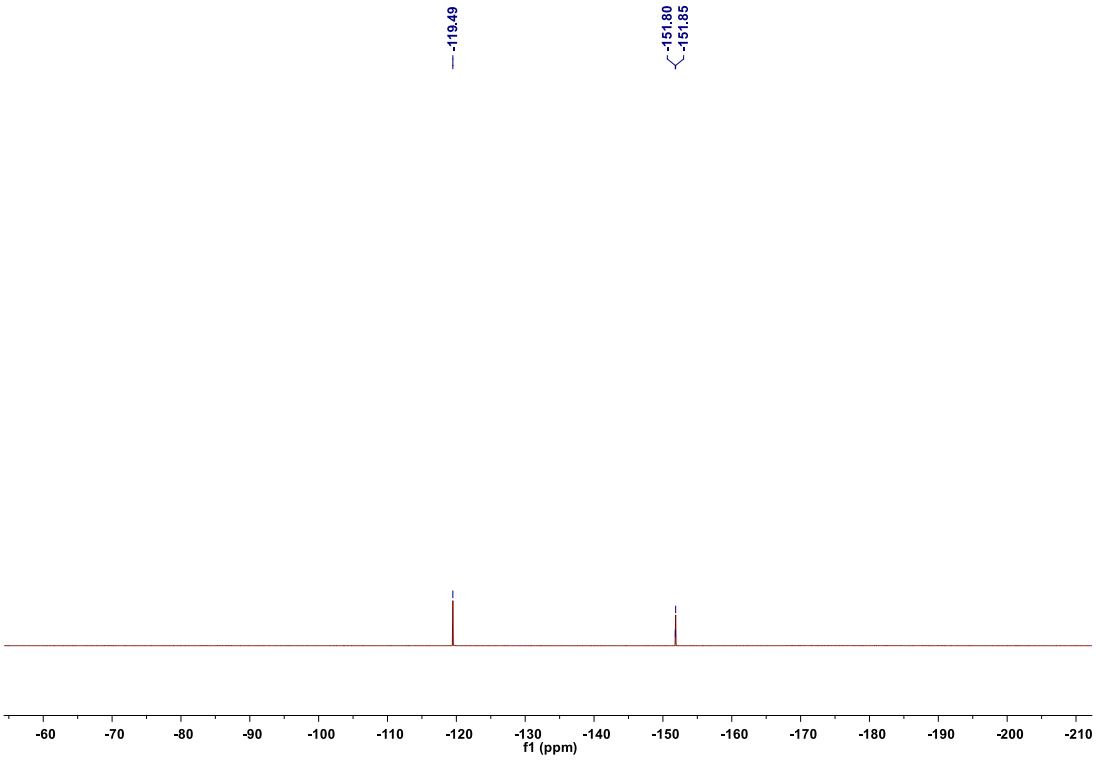

^{19}F NMR spectrum (564 MHz, CD_3CN, 298 K) of compound **8**.

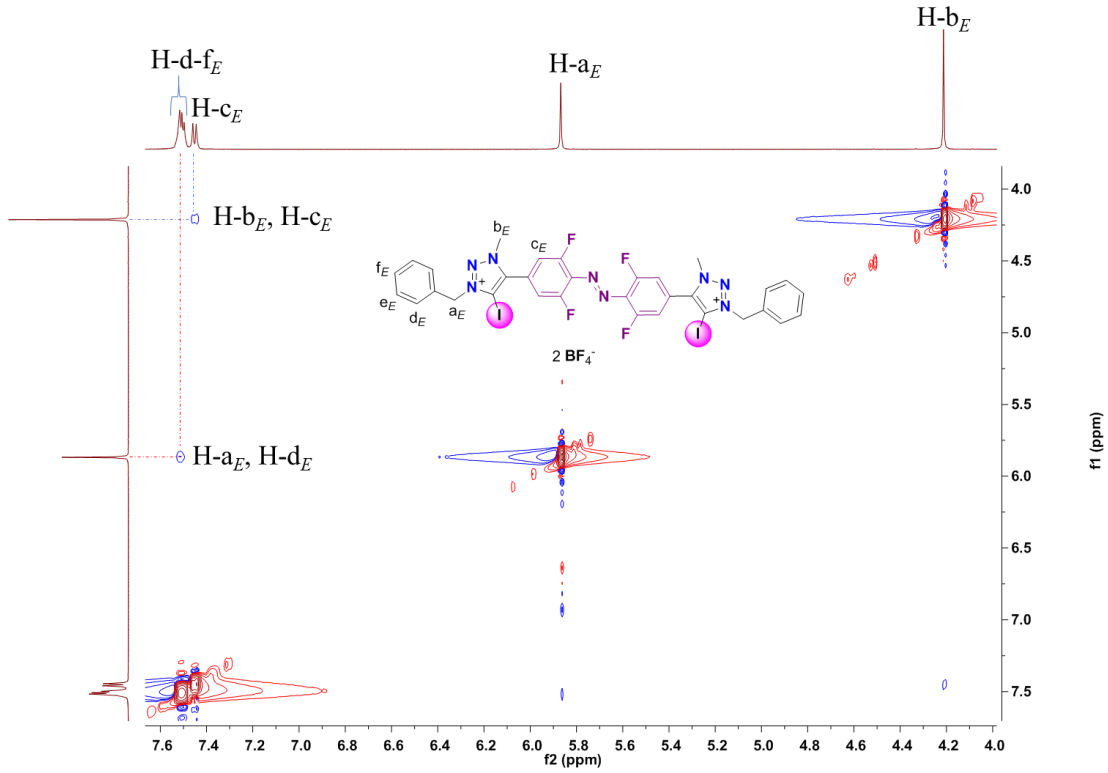

2D NOSEY-NMR spectrum (600 MHz, 10 mM, CD_3CN, 298 K) of compound **8**.

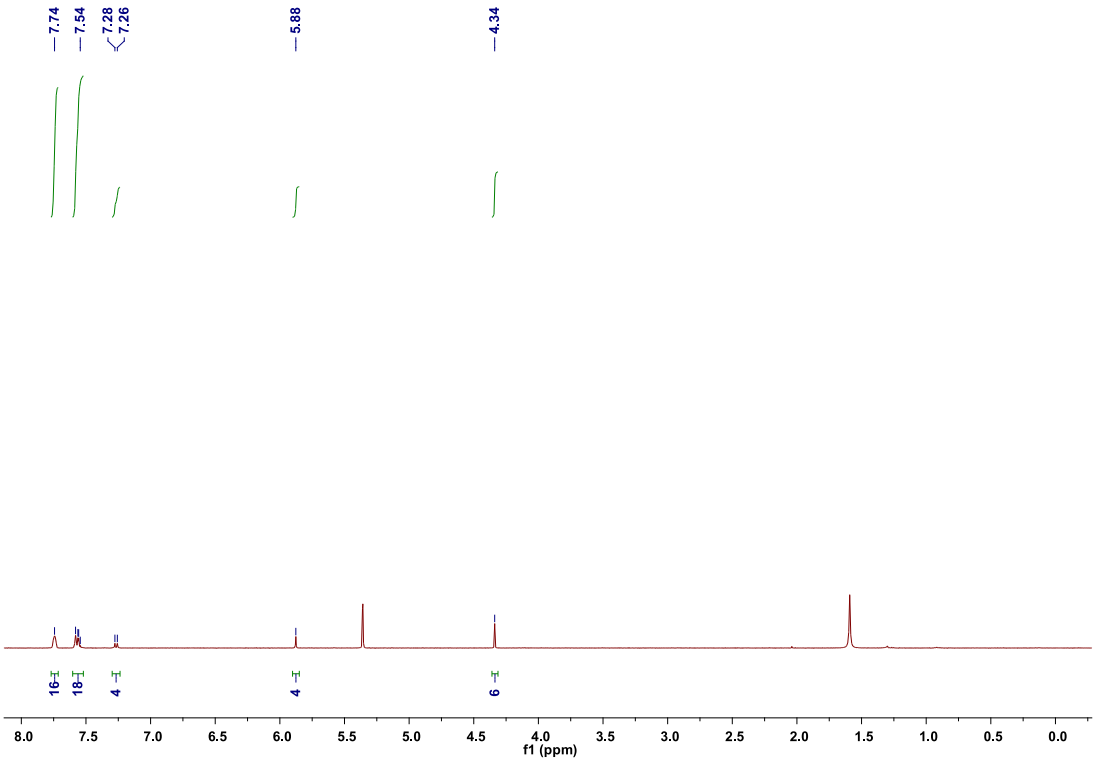

^{1}H NMR spectrum (400 MHz, CD_2Cl_2, 298 K) of compound **XB-1**.

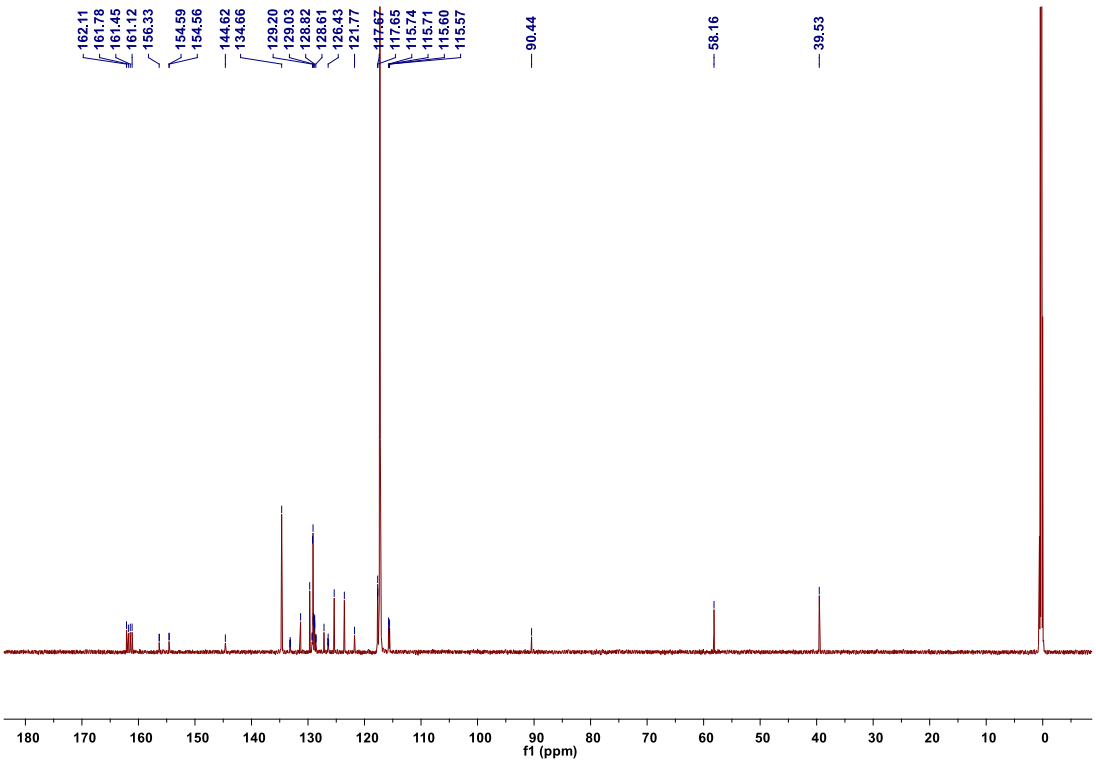

^{13}C NMR spectrum (150 MHz, CD_3CN, 298 K) of compound **XB-1**.

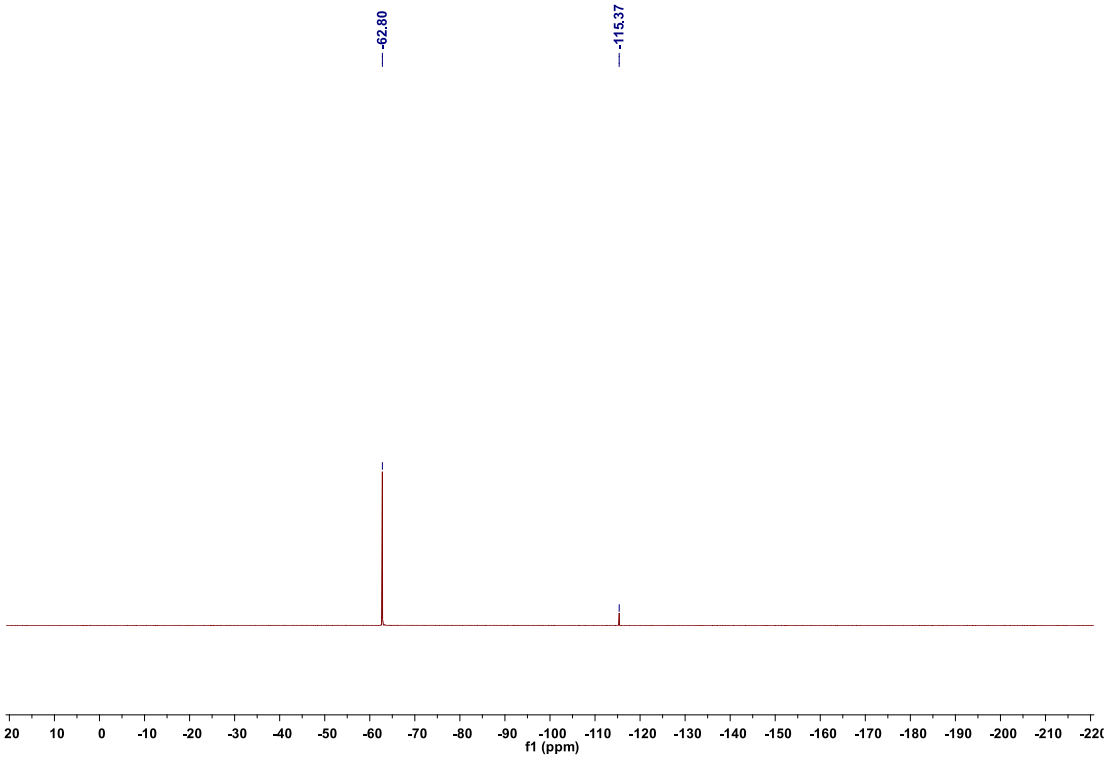

^{19}F NMR spectrum (376 MHz, CD_2Cl_2, 298 K) of compound **XB-1**.

References

[1] H.-Y. Duan, S.-T. Han, T.-G. Zhan, L.-J. Liu and K.-D. Zhang, *Angew. Chem., Int. Ed.*, 2023, **62**, e202212707.

[2] http://supramolecular.org

[3] B. Hibbert and P. Thordarson. *Chem. Commun.*, 2016, **52**, 12792-12805.

[4] R. Haraguchi, T. Nishikawa, A. Kanazawa and S. Aoshima, *Macromolecules*, 2020, **53**, 4185-4192.